Schweizerische Eidgenossenschaft
Confédération suisse
Confederazione Svizzera
Confederaziun svizra

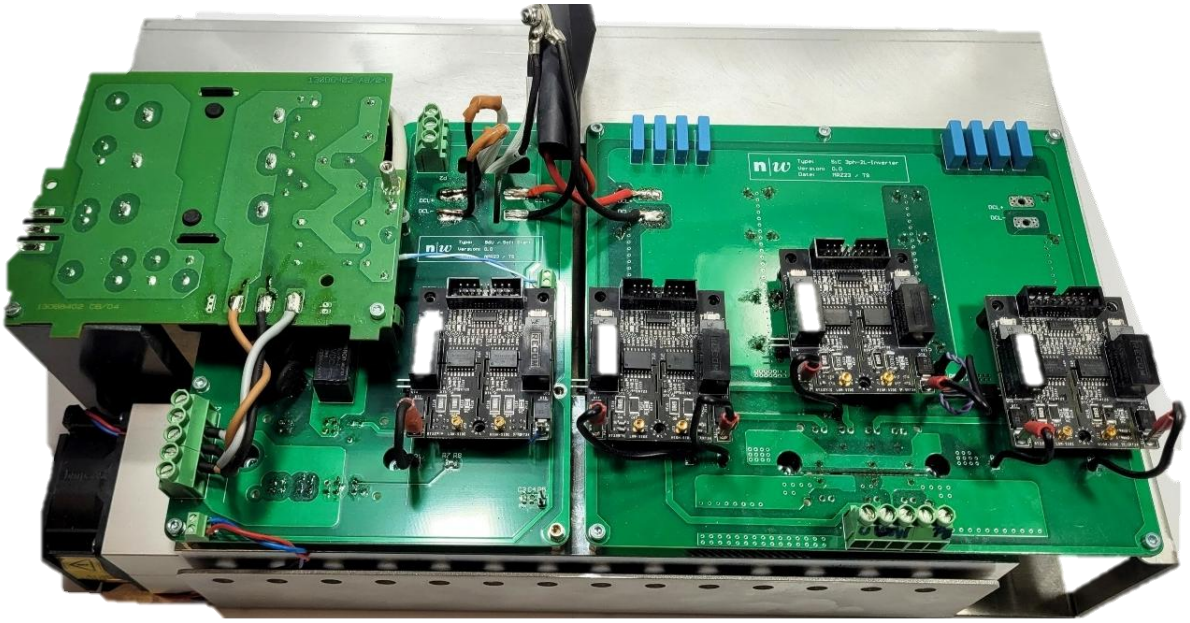
Federal Department of the Environment,
Transport, Energy and Communications DETEC

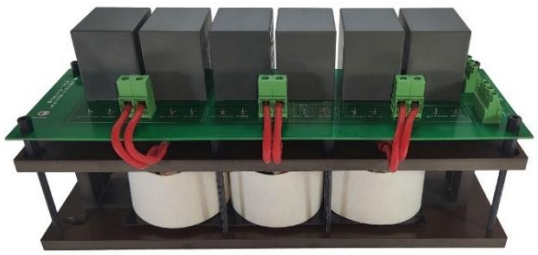
Swiss Federal Office of Energy
Energy Research and Cleantech

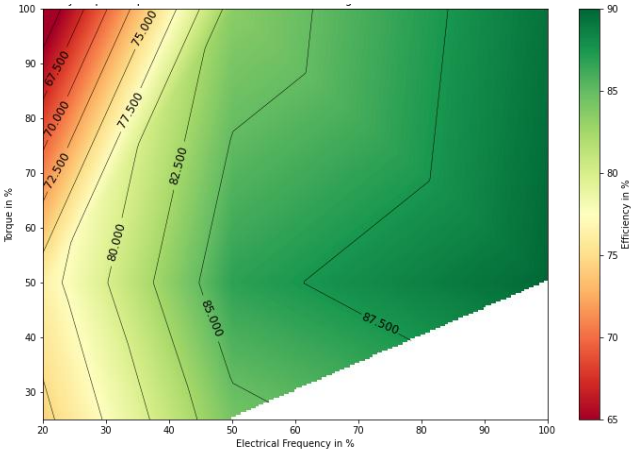
Final report from 28 May 2025

OPTIPUMP

Optimal application-relevant system efficiency of SiC pump drives







Source: FHNW, 2025

University of Applied Sciences and Arts Northwestern Switzerland
School of Engineering and Environment

Publisher:
Swiss Federal Office of Energy SFOE
Energy Research and Cleantech
CH-3003 Berne
www.energy-research.ch

Subsidy recipients:
University of Applied Sciences and Arts Northwestern Switzerland FHNW
School of Engineering and Environment
Institute of Electric Power Systems
Klosterzelgstrasse 2
CH-5210 Windisch

https://www.fhnw.ch/en/about-fhnw/schools/school-of-engineering/institutes/institute-of-electric-power-systems

Authors:
Tobias Strittmatter, FHNW, tobias.strittmatter@fhnw.ch
Dr. Christian Stamm, FHNW, christian.stamm@fhnw.ch
Silvan Rehm, previously FHNW
Prof. Dr. Nicola Schulz, FHNW, nicola.schulz@fhnw.ch

SFOE project coordinators:
Dr. Michael Moser, michael.moser@bfe.admin.ch
Roland Brüniger, roland.brueniger@brueniger.swiss

SFOE contract number: SI/502411-01

The authors bear the entire responsibility for the content of this report and for the conclusions drawn therefrom.

Language and Translation Note

Some sections of this report are based on previous annual reports originally written in German. These parts have been translated into English with the assistance of DeepL. In addition, the French and German summaries were also translated using DeepL. While all translations have been carefully reviewed, minor deviations in phrasing or tone may occur due to the automated nature of the translation process.

To improve clarity and readability, selected parts of the English version were further refined using AI-based language tools (Grammarly, ChatGPT). These tools were solely used for stylistic enhancement. All content, including interpretations and conclusions, originates exclusively from the authors.

Summary

The objective of this project is to compare a commercial 5.5 kW electrical standard drive system for pumps utilizing IGBT technology with a SiC MOSFET-based drive system developed at FHNW. Both systems feature a two-level, three-phase voltage source inverter topology and are powered by a three-phase diode bridge rectifier. The comparison focuses on efficiency and energy losses under realistic operating conditions, which frequently occur at partial load. Efficiency measurements were conducted in accordance with the IEC 61800-9-1 standard. All measurements were executed on complete drive systems, which also include the grid-side filter, control electronics, motor-side filter, and motor.

The specifications of the frequency converter developed at the FHNW were adopted directly from the reference system of the manufacturer Grundfos to ensure direct comparability. Key components of the developed SiC converter are:

- Diode rectifier module (silicon-based)
- SiC MOSFET 3-phase full-bridge module
- Grid-side filter and DC choke, used from the reference system.
- Own-developed motor-side sine-wave filter incorporating Kool-Mu core material

A test bench for drive systems was set up from the ground up to carry out the efficiency measurements. The test bench can apply torque and speed to the motor of the system under test to systematically approach target operating points. The efficiency measurements were conducted in accordance with IEC 61800-9-1, specifically from the mains connection to the motor shaft using a precision power analyser. Additional measurements were performed to gain a deeper understanding of the distribution of losses in the drive system.

The key results of the efficiency comparison are:

- Changing from IGBT-based inverters to SiC MOSFETs results in a system efficiency increase of up to 10 percentage points in partial load and 1 percentage point in nominal load.
- Higher switching frequency than the standard value of 8 kHz does not reduce overall losses, whether with or without a sine wave motor filter at the output of the frequency converter.
- Implementing a motor-side filter with low-loss core material increases the efficiency further and, in combination with a SiC inverter, reduces total system losses to a minimum.
- Removing the sine wave filter increases the losses, since the losses occurring in the motor increase disproportionately due to the unfiltered current ripple.

Based on the energy loss data gathered for the two drive systems, an estimate was made regarding the potential global energy savings that could be achieved if all speed-controlled drive systems were transitioned to SiC technology. The estimated annual global energy savings from SiC drives in pump applications range from 17 TWh to 25 TWh.

To assist users of drive systems in evaluating their energy consumption based on their specific operating profiles, a calculation tool has been developed and is available online for interested users. By entering a dataset that includes their operating profiles and efficiency data, users can calculate their energy consumption and make comparisons between different drive systems.

Zusammenfassung

In diesem Projekt wird ein kommerzielles 5.5 kW Antriebssystem für Pumpen mit IGBT-Technologie mit einem an der FHNW entwickelten SiC MOSFET-basierten Antriebssystem verglichen. Beide Systeme verfügen über eine 2-Level, dreiphasige Wechselrichter-Topologie und werden von einem dreiphasigen Diodenbrücken-Gleichrichter gespeist. Im Zentrum des Vergleichs stehen der Wirkungsgrad und die energetischen Verluste unter realistischen Betriebsbedingungen, die häufig im Teillastbereich stattfinden. Die Wirkungsgradmessungen wurden in Übereinstimmung mit der Norm IEC 61800-9-1 durchgeführt. Alle Messungen wurden an kompletten Antriebssystemen durchgeführt, die auch den netzseitigen Filter, die Steuerelektronik, den motorseitigen Filter und den Motor beinhalten.

Die Spezifikationen des an der FHNW entwickelten Frequenzumrichters wurden direkt vom Referenzsystem des Herstellers Grundfos übernommen, um eine direkte Vergleichbarkeit zu gewährleisten. Die wichtigsten Komponenten des entwickelten SiC-Umrichters sind:

- Dioden-Gleichrichtermodul (auf Siliziumbasis)
- SiC MOSFET 3-Phasen-Vollbrückenmodul
- Netzseitiger Filter und DC-Drossel, die aus dem Referenzsystem übernommen wurden.
- Eigenentwickelter motorseitiger Sinusfilter mit Kool-Mu Kernmaterial

Für die Durchführung der Wirkungsgradmessungen wurde ein Prüfstand für Antriebssysteme von Grund auf neu aufgebaut. Mit dem Prüfstand kann der Motor des zu testenden Systems mit Drehmoment und Drehzahl beaufschlagt werden, um systematisch die gewünschten Betriebspunkte anzufahren. Die Wirkungsgradmessungen wurden gemäss IEC 61800-9-1 durchgeführt, d.h. vom Netzanschluss bis zur Motorwelle mit einem Präzisions-Leistungsmessgerät. Zusätzliche Messungen wurden durchgeführt, um ein tieferes Verständnis über die Verteilung der Verluste im System zu erhalten.

Die wichtigsten Ergebnisse des Effizienzvergleichs sind:

- Der Wechsel von IGBT-basierten Umrichtern zu SiC-MOSFETs führt zu einer Steigerung des Systemwirkungsgrads von bis zu 10 Prozentpunkten unter Teillast und 1 Prozentpunkt bei Nennlast.
- Eine höhere Schaltfrequenz als der Standardwert von 8 kHz führt nicht zu einer Verringerung der Gesamtverluste, weder mit noch ohne Sinusfilter am Ausgang des Frequenzumrichters.
- Die Implementierung eines motorseitigen Filters mit verlustarmem Kernmaterial erhöht den Wirkungsgrad weiter und reduziert in Kombination mit einem SiC-Umrichter die Gesamtsystemverluste auf ein Minimum.
- Das Entfernen des Sinusfilters erhöht die Verluste, da die im Motor auftretenden Verluste durch die ungefilterte Stromwelligkeit überproportional ansteigen.

Auf der Grundlage der für die beiden Antriebssysteme gesammelten Energieverlustdaten wurde eine Schätzung der potenziellen globalen Energieeinsparungen vorgenommen, die erzielt werden könnten, wenn alle drehzahlgeregelten Antriebssysteme auf die SiC-Technologie umgestellt würden. Die geschätzten jährlichen weltweiten Energieeinsparungen durch SiC-Antriebe in Pumpenanwendungen lieben im Bereich zwischen von 17 TWh bis 25 TWh.

Um die Nutzer von Antriebssystemen bei der Bewertung des Energieverbrauchs bei ihren spezifischen Betriebsprofilen zu unterstützen, wurde ein Berechnungstool entwickelt, das interessierten Nutzern online zur Verfügung steht. Durch Eingabe eines Datensatzes, der ihre Betriebsprofile und Effizienzdaten enthält, können die Nutzer ihren Energieverbrauch berechnen und Vergleiche zwischen verschiedenen Antriebssystemen anstellen.

Résumé

L'objectif de ce projet est de comparer un système commercial d'entraînement électrique standard de 5,5 kW pour les pompes utilisant la technologie IGBT avec un système d'entraînement basé sur le SiC MOSFET développé à la FHNW. Les deux systèmes présentent une topologie d'onduleur à source de tension triphasée à deux niveaux et sont alimentés par un pont redresseur à diodes triphasé. La comparaison porte sur le rendement et les pertes d'énergie dans des conditions de fonctionnement réalistes, qui se produisent fréquemment à charge partielle. Les mesures de rendement ont été effectuées conformément à la norme IEC 61800-9-1. Toutes les mesures ont été effectuées sur des systèmes d'entraînement complets, qui comprennent également le filtre côté réseau, l'électronique de commande, le filtre côté moteur et le moteur.

Les spécifications du convertisseur de fréquence mis au point à la FHNW ont été adoptées directement à partir du système de référence du fabricant Grundfos afin d'assurer une comparabilité directe.

Les principaux composants du convertisseur SiC développé sont les suivants :

- Module redresseur à diodes (à base de silicium)
- Module de pont complet triphasé à MOSFET SiC
- Filtre côté réseau et self CC, utilisés dans le système de référence.
- Filtre sinusoïdal côté moteur développé par nos soins et incorporant le matériau de base Kool-Mu.

Un banc d'essai pour les systèmes d'entraînement a été mis au point pour effectuer les mesures d'efficacité. Le banc d'essai peut appliquer un couple et une vitesse au moteur du système testé pour s'approcher systématiquement des points de fonctionnement cibles. Les mesures de rendement ont été effectuées conformément à la norme CEI 61800-9-1, en particulier entre la connexion au réseau et l'arbre du moteur, à l'aide d'un analyseur de puissance de précision. Des mesures supplémentaires ont été effectuées pour mieux comprendre la répartition des pertes dans le système d'entraînement.

Les principaux résultats de la comparaison des rendements sont les suivants :

- Le passage des convertisseurs à base d'IGBT aux MOSFET SiC entraîne une augmentation de l'efficacité du système pouvant atteindre 10 points de pourcentage à charge partielle et 1 point de pourcentage à charge nominale.
- Une fréquence de commutation supérieure à la valeur standard de 8 kHz n'entraîne pas de réduction des pertes totales, que ce soit avec ou sans filtre sinusoïdal à la sortie du variateur de fréquence.
- La mise en œuvre d'un filtre côté moteur avec un matériau de noyau à faibles pertes augmente encore le rendement et, en combinaison avec un convertisseur SiC, réduit les pertes totales du système à un minimum.
- La suppression du filtre sinusoïdal augmente les pertes, car les pertes qui se produisent dans le moteur augmentent de manière disproportionnée en raison de l'ondulation de courant non filtrée.

Sur la base des données relatives aux pertes d'énergie recueillies pour les deux systèmes d'entraînement, nous avons estimé les économies d'énergie potentielles au niveau mondial qui pourraient être réalisées si tous les systèmes d'entraînement à vitesse variable étaient convertis à la technologie SiC. Les économies d'énergie annuelles estimées au niveau mondial grâce aux entraînements SiC dans les applications de pompage se situent dans une fourchette de 17 TWh à 25 TWh.

Pour aider les utilisateurs de systèmes d'entraînement à évaluer leur consommation d'énergie en fonction de leurs profils de fonctionnement spécifiques, un outil de calcul a été développé et est disponible en ligne pour les utilisateurs intéressés. En entrant un ensemble de données comprenant leurs profils de fonctionnement et leurs données d'efficacité, les utilisateurs peuvent calculer leur consommation d'énergie et faire des comparaisons entre différents systèmes d'entraînement.

Main findings («Take-Home Messages»)

- Optimising the efficiency of a drive system specifically for the partial load range is important because in practice many drive systems are only operated at partial load.
- In comparison to IGBT-based electric drive systems (kW power range), the use of SiC MOSFETs in the inverter enables significant efficiency improvement, mainly in the partial load regime.
- The efficiency of an own-developed 5.5 kW SiC drive system was measured to be 1.3 percentage points (nominal load region) to 10 percentage points (partial load) higher than a comparable IGBT-based drive system.
- The optimal efficiency of the SiC drive system was obtained at the lowest tested switching frequency of 8 kHz.
- A frequency converter based on SiC MOSFETs is not more complex than an IGBT inverter. It should be aimed for a DC link with low parasitic inductance.
- For a more conservative design regarding the voltage slopes, SiC MOSFETs can also be operated at a lower dV/dt comparable to IGBTs, since the majority of losses occurs in the filter and in the motor.
- To design a drive system for optimal efficiency, also additional components such as the motor-side sine-wave filter should be taken into account.
- The global energy-saving potential of SiC drive systems for pumps in the kW power range is estimated to 17 – 25 TWh/a.

Contents

Language and Translation Note ... **3**
Summary ... **4**
Zusammenfassung ... **5**
Résumé ... **6**
Main findings («Take-Home Messages») ... **7**
Contents ... **8**
List of abbreviations ... **10**
Introduction ... **11**
1.1 Context ... 11
1.2 Motivation ... 11
1.3 Project objectives ... 12
Investigated commercial pump drive system ... **13**
2.1 Definition and takeover of the pump drive system ... 13
2.2 Requirements for characterising the Grundfos system ... 15
Test bench for drive systems ... **18**
3.1 Hardware ... 18
3.2 IT components and software ... 18
Basic characterisation of the Grundfos pump drive system ... **21**
4.1 System boundaries for the efficiency measurements ... 21
4.2 Frequency converter (CUE 3 x 380-500V IP20 5.5kW) ... 22
4.3 Output filter ... 24
4.4 MG132SC induction motor ... 27
Development of the SiC converter prototype ... **29**
5.1 Definition of requirements specifications ... 29
5.2 PLECS Simulation Model ... 31
5.3 Selection of components ... 32
5.4 Mechanical Concept ... 36
Development of the motor-side filter ... **38**
6.1 Influence of the current ripple on the losses ... 38
6.2 Initial tests of the filter ... 42
Efficiency and loss measurements ... **43**
7.1 Measurement setup ... 43
7.2 Measurement procedure ... 43
7.3 Measurement uncertainties ... 44
7.4 Grundfos variable speed drive with commercial filter ... 46
7.5 SiC variable speed drive with commercial filter ... 47

7.6 SiC variable speed drive with Kool-Mu filter 48
Conclusions from the measurements 49
8.1 Efficiency comparison 49
8.2 Impact of the switching frequency on SiC PDS losses 51
8.3 SiC VSD without sine filter at different switching frequencies 53
8.4 Conclusion 56
Energetic considerations of Si and SiC pump drives 57
9.1 Calculating energic losses for given mission profiles 57
9.2 Determination of real pump operating profiles 59
9.3 Global energy demand of speed-controlled pumps 61
9.4 Conversion of power to torque and speed for hydraulic systems 62
9.5 Energy and cost saving potential per 5.5 kW system 63
9.6 Annual global energy saving potential of SiC pump drives 64
Online tool for energetic calculations 65
10.1 Intended purpose 65
10.1 Implementation and functions 66
Conclusions and outlook 67
11.1 Conclusions 67
11.2 Outlook 68
National and international cooperation 69
12.1 Grundfos Pumpen AG 69
12.2 Plexim GmbH 69
Publications and other communications 70
References 71

List of abbreviations

AC	Alternating current
CDM	Complete drive module
DAB	Dual active bridge
DC	Direct current
EMC	Electro-magnetic compatibility
ESR	Equivalent series resistance
FC	Frequency converter
FHNW	University of Applied Sciences and Arts Northwestern Switzerland
IEC	International Electrotechnical Commission
IGBT	Insulated gate bipolar transistor
IT	Information technology
LAN	Local area network
MOSFET	Metal oxide semiconductor field effect transistor
PC	Personal computer
PDS	Power drive system
PWM	Pulse width modulation
SFOE	Swiss Federal Office of Energy
Si	Silicon
SiC	Silicon carbide
UI	user interface
VSD	variable speed drive

Introduction

1.1 Context

Silicon carbide (SiC) frequency converters in the power range of a few kW can offer great energy-saving potential in speed-controlled pump drives, ventilation systems, hydraulic systems or conveyor systems such as lifts and escalators. This potential can be attributed to the low switching and conduction losses of SiC MOSFETs compared to silicon power semiconductors. The high efficiency of SiC MOSFETs, especially in the partial load range, was demonstrated by the FHNW in a dual active bridge (DAB) converter in the SFOE-funded 'SiCUm' project [1].

In addition to the power semiconductors, there are numerous other components and subsystems in an operational inverter that influence the overall efficiency relevant to the application (or the resulting total energy requirement over a period of time):

- Magnetic components such as chokes and transformers,
- Auxiliary supplies for the control of semiconductors and relays, as well as for measurements and their data processing,
- Displays and user interfaces,
- Gate drivers for power semiconductors: higher switching frequency leads to higher power consumption,
- Fans / pumps for cooling (higher system losses leads to higher fan or pump power),
- Losses to resistors in capacitors in intermediate and snubber circuits (balancing of capacitors) and protective circuits (varistors),
- Necessary filters to fulfil application-specific standards.

In 10 kW systems, which are operated with 95% efficiency at their nominal point, these losses easily amount to more than 50 W and thus a further 0.5%. In partial load operation, their share of the total losses increases disproportionately.

Furthermore, if a motor is operated by a SiC inverter with a high switching frequency (> 10 kHz) or high dV/dt to minimise switching losses, additional effects in the motor may have to be taken into account, which influence both the feasibility and the overall efficiency of the system. For example, high-frequency current harmonics cause additional losses that thermally limit the possible output power of the machine and reduce efficiency. To suppress these harmonics, output filters can be used, which in turn cause further losses.

1.2 Motivation

Depending on the load profile (proportion of full load / partial load operation) of a drive system, the energy consumption over a period of time results from the individual consumptions of the subsystems and components mentioned above. The switching frequency of the power transistors is expected to have an impact on this overall energy requirement. This project therefore aims to investigate to what extent and how the switching frequency, as well as other parameters, can be selected to optimise the overall application-relevant energy requirement of a drive system.

For this purpose, the efficiency behaviour of a SiC drive system is systematically investigated and its overall energy requirement is optimised for typical pump application profiles. The drive system includes the power converter and the machine, as well as all components and subsystems required for operation. The investigations and optimisations are carried out experimentally by means of parameter variation on a SiC pump drive, whereby the SiC converter is developed at the FHNW. A commercial pump drive system provided by Grundfos Pumpen AG serves as a reference system with conventional silicon IGBT technology.

Based on the experimental findings regarding the efficiencies, the energy-saving potential of SiC pump drives for typical application profiles is derived. Due to the database and experimentally validated calculations, a higher accuracy of the determined energy saving potential is expected than in previous estimates (e.g. [2]).

1.3 Project objectives

Based on the motivation, these **research questions** are to be answered:

1. How much energy can be saved annually by a SiC pump drive optimised in terms of its application relevant overall efficiency in the power range of a few kW compared to a conventional silicon-based system for a typical pump application profile?
2. What is the energy saving potential in the optimum case compared to commercial silicon-based speed-controlled drives for the pump applications analysed?
3. What design recommendations can be given to manufacturers who wish to convert their Si inverter of a variable speed pump drive to SiC for a lower overall energy requirement?

The following **project objectives** serve to answer the research questions:

1. Characterisation of a commercial, silicon-based pump drive in the kW range (system limits: mains connection to the motor shaft) in terms of its efficiency in accordance with IEC 61800-9-2 and determination of its annual energy requirement for at least one typical pump application profile.
2. Development of a SiC inverter with the highest possible efficiency and with comparable functional and performance data to the silicon reference system from the project objective.
3. Characterisation of the SiC converter in terms of its efficiency in accordance with IEC 61800-9-2 [3] for three different switching frequencies, with hardware (e.g. filters) and control adapted to the respective switching frequency.
4. Development of a calculation tool that calculates the total energy losses of the inverter and the machine for specified application profiles, as well as inverter and machine parameters, and that can be used to optimise the inverter in terms of its energy requirements.

Investigated commercial pump drive system

2.1 Definition and takeover of the pump drive system

This project is about evaluating the potential energy savings by improving the pump system efficiency. By estimating a typical load profile of the application and the corresponding market volume of the system, it can be realistically estimated how much energy can be saved with a SiC-based pump system compared to the state-of-the-art solution.

A suitable, widely used pump family was therefore selected together with Grundfos Pumpen AG, which fulfils the following basic requirements:

1. It should be a speed-controlled drive system with frequency converter, motor, pump and associated mains and sinusoidal filters.
2. The power range should be in the < 22 kW range.
3. The pump family should have the largest possible market volume.
4. Typical load profiles should be available, e.g. flow rate / time (with associated pump characteristic curve) or torque and speed of the motor shaft / time.

Chosen was the NK / NKE standard pump family (Figure 1 and Figure 2), being suitable for a wide range of applications.



Figure 1: Grundfos NK, NKE standard pumps [4].

Table 1: Suitable applications for the NK / NKE pump family.

Heating for commercial properties	Pressure boosting for commercial properties
District cooling	Drinking water treatment
District heating	Cooling
Irrigation	Heating systems in industrial plants
Desalination	Transport of process fluids
Machining	Water supply
Industrial process water treatment	Surface water extraction
Water distribution in waterworks	Municipal waste water treatment

To determine the specific type, the availability of suitable variants was checked. In the end, the following pump system was selected. The assemblies can be found in Table 1.



Figure 2: Grundfos NK pump K 32-160/177 AA2F2AESBQQELW1 [4].

This type (combination of inverter, filter, motor) is representative of the NK pump family with frequency inverter control. This means that the findings and statements from the project can be applied qualitatively to the other NK pumps.

Table 2: Components of the variable speed pump system from Grundfos.

Component	Product name	Product number	Reference
Frequency inverter	CUE 3 x 380-500V IP20 5,5kW	99616714	[5]
Sinusoidal filter	Sine-wave filter	96754976	[6]
Motor	MG132SC	87322374	[7]
Pump	NK 32-160/177 AA2F2AESBQQELW1	98973410	[4]

2.2 Requirements for characterising the Grundfos system

The energy efficiency of the drive system (“PDS” in Figure 3) is determined in accordance with the IEC 61800-9-1 standard [8]. For this purpose, a test bench has been set up at the Institute for Electrical Power Systems at the FHNW for this purpose (see Chapter 0).

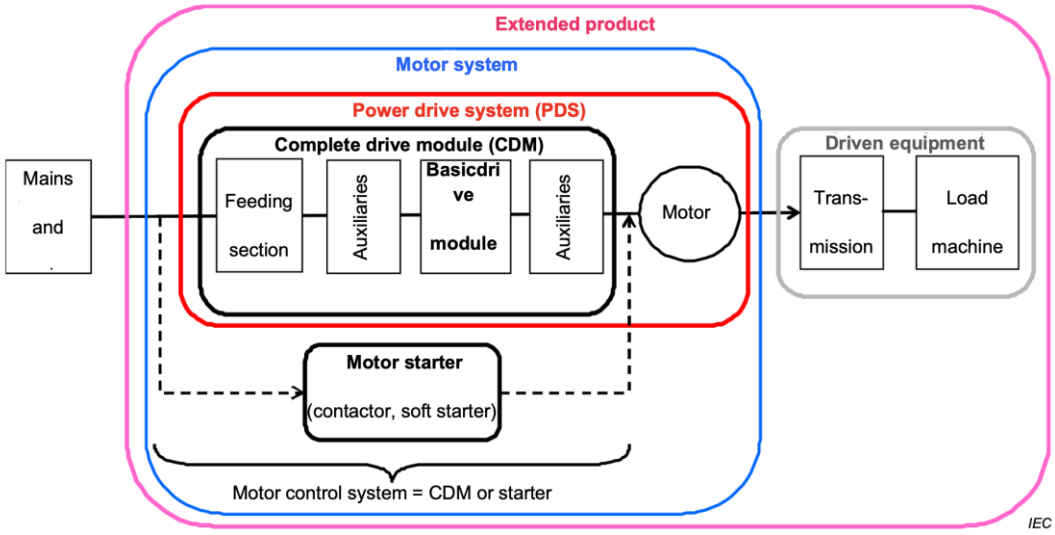


Figure 3: System boundaries of the extended product range according to IEC 61800-9-1. The area framed in red is relevant for this project [8].

For the reference system provided by Grundfos, this means that the hydraulic pump is uncoupled from the motor shaft. The motor is coupled to a load machine on the test bench, with which the operating points shown in Figure 4 below, torque at one speed, are approached.

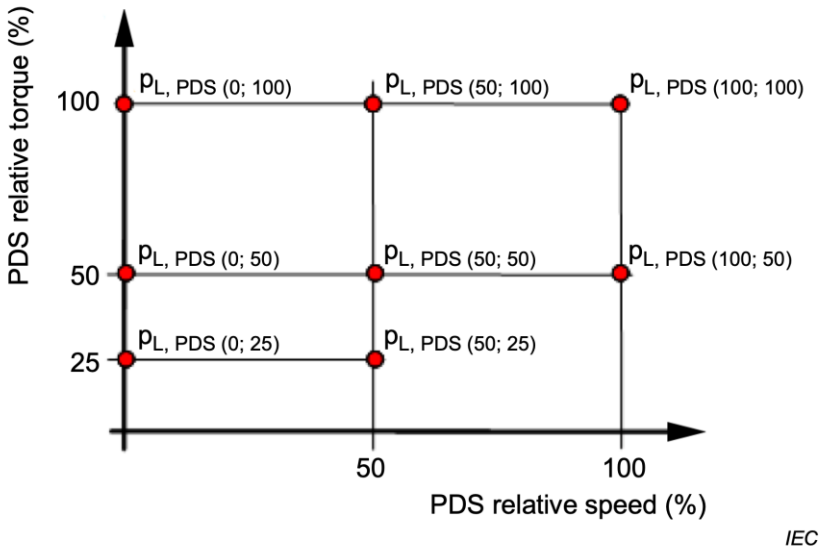


Figure 4: Visualisation of the operating points (shaft speed, torque) to determine the relative losses of the drive system (PDS) [8].

The system efficiency is measured at the operating points from the three-phase 400 VAC mains to the motor shaft. The measurement system shown in Figure 5 is used for this purpose. It simultaneously records the six electrical input variables (U1, I1, U2, I2, U3, I3) as well as the torque and speed of the motor shaft and calculates the loss power and efficiency.



Figure 5: HIOKI PW8001 Power Analyser with calibrated current transducers [9].

Table 3: Measuring system for motor test bench for direct determination of energy efficiency.

Device	Product number	Description	Reference
HIOKI Analyser	PW8001-11	Power analyser - modular system, DC, 0.1 Hz – 5 MHz with motor analysis	[10]
HIOKI measurement board	U7005	Modul für PW8001 - 5 MHz, 15 MS/s, 1'000 V AC/DC, bis 2'000 A with transducers, 18-bit Measurement inaccuracy (power at 50/60 Hz): ±0.03%	[10]
HIOKI current transducer	CT6872	AC/DC Current sensor, frequency bandwidth: DC to 10 MHz, 50 A AC/DC Amplitude inaccuracy (50/60 Hz): ±0.03% of rdg. (measured value), ±0.007% f.s. (measurement range) Automatic phase correction by PW8001	[10]
Shaft torque sensor	4503A100L0000000	Manufacturer: Kistler (MTS)	[11]

The torque and speed are measured with a torque shaft of type Kistler 4503A100L torque sensor with the accuracy specified in Table 4.

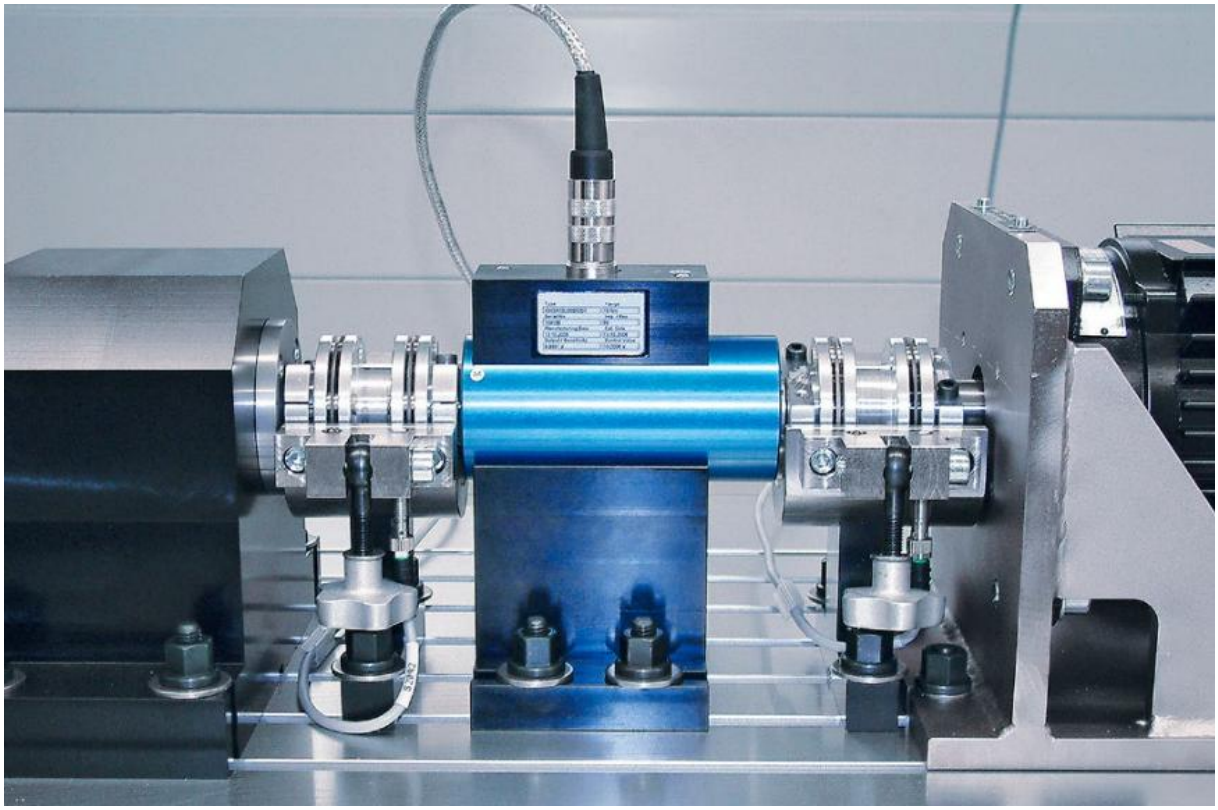


Figure 6: Shaft torque sensor Kistler 4503A100L0000000 [11].

Table 4: Accuracies EN 60034-2-1 vs. Kistler 4503A100L0000000 torque measuring shaft.

Parameter	Accuracy specification EN 60034-2-1	Torque measuring shaft accuracy
Accuracy class Torque measurement	0.2	0.1
Speed measurement	≤ 0.1 1/min	60 imp./rev.
Temperature influence on the measuring accuracy	should be limited to 0.15 % of the measuring range	0.005 % / °C on zero point 0.01 % / °C on nominal value

The temperature influence is 0.15 % / degree Celsius for the used sensor. A temperature change of the sensor higher than 30 K is not expected, as all measurements are carried out in an air-conditioned room at approx. 20 - 25°C.

Test bench for drive systems

3.1 Hardware

The Grundfos and FHNW-SiC drive systems are to be compared with each other on a drive test bench in terms of their overall efficiency at the same operating points (torque, speed). The system limits are the grid connection (measurement of the electrical power drawn from the 400 V grid) and the motor shaft (measurement of the mechanical power output). These electrical and mechanical variables are measured simultaneously using sensors and a power analyser (see section 2.2).

The operating points are controlled with a load machine, which is operated via its own variable speed drive (VSD). The load machine with VSD is used from the institute's own stock. The machines are mounted on a table with their shafts running in the same alignment. The two machines are coupled via the torque measuring shaft, see [11].

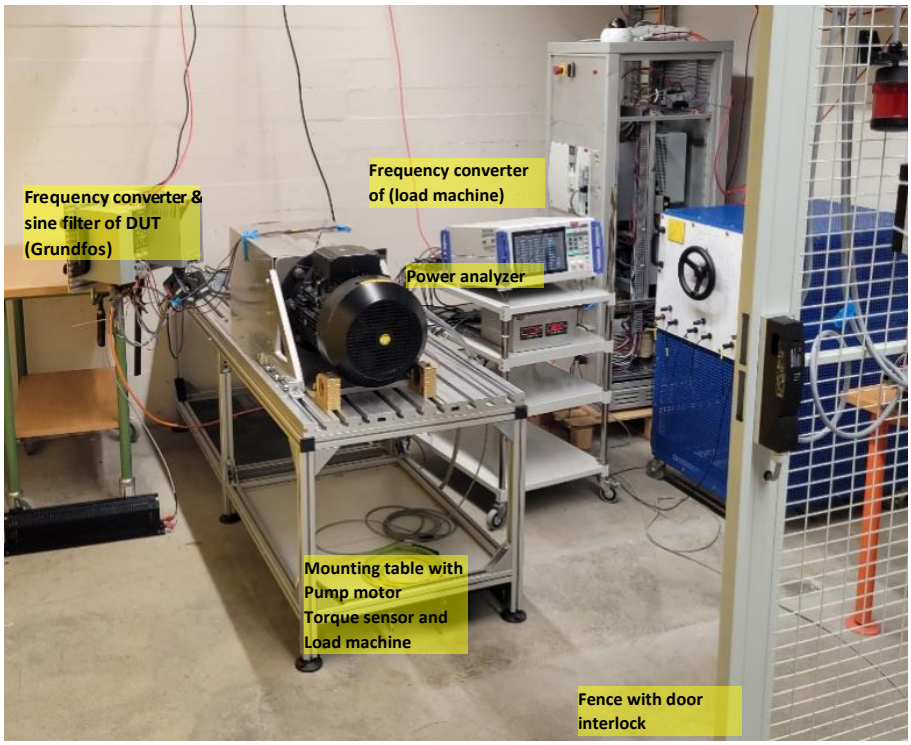


Figure 7: Photo of the test bench for drive systems at FHNW.

The entire setup is placed inside a fenced area and can be remotely controlled for personal safety. During the test run the access door is interlocked for prevention to touch devices under voltage or with a rotating.

3.2 IT components and software

The test bench IT components and software, are briefly described below:

Network architecture

For safety reasons, the test setup is installed in a sealed test cell. Communication with the outside world takes place via an optical fibre, so the user is galvanically isolated from the setup. A PC is in the test cell, which both controls the system and collects data. The two inverters are controlled via an analogue

voltage, which is provided by a ‘LabJack’. The measurement data is generated by the Power Analyser. Like the LabJacks, it is connected to the PC via LAN, as shown in Figure 8.

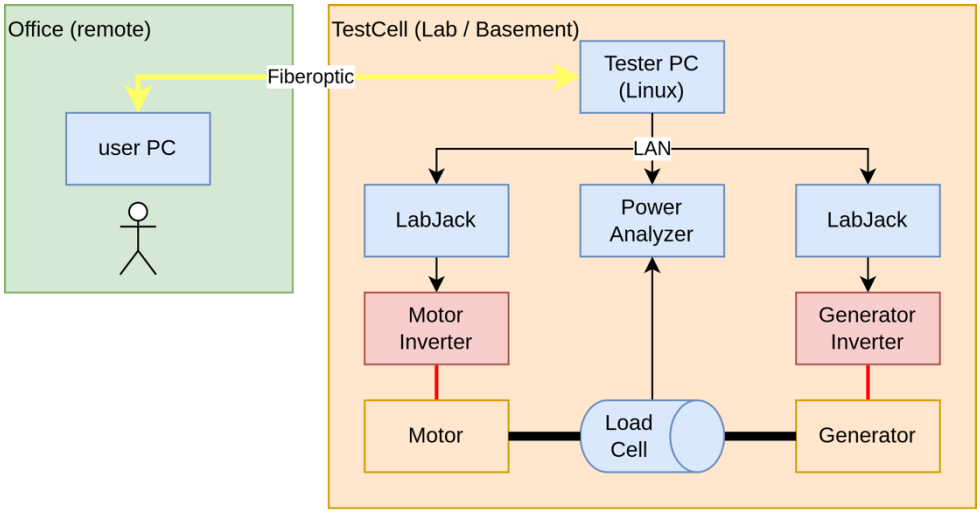


Figure 8: Architecture of the test bench.

Software architecture

The software consists of two parts: A user interface (UI), which runs at the system user's location, and a tester part (orange in Figure 9). The UI is connected to the server PC in the test cell. It retrieves current values from the test system via a socket and displays them. New operating points are transmitted from the UI to the server. This sends them internally to a controller on which an internal state machine is running (see Figure 10). The controller sets new values for the inverters and saves these in the ‘data_hub’, a central data storage location. The Power Analyser has an internal thread that regularly collects new measured values and saves them in the data_hub. The ‘periodicCSVLogger’ is used to record the data. This writes the values from the data_hub to a CSV file at regular intervals.

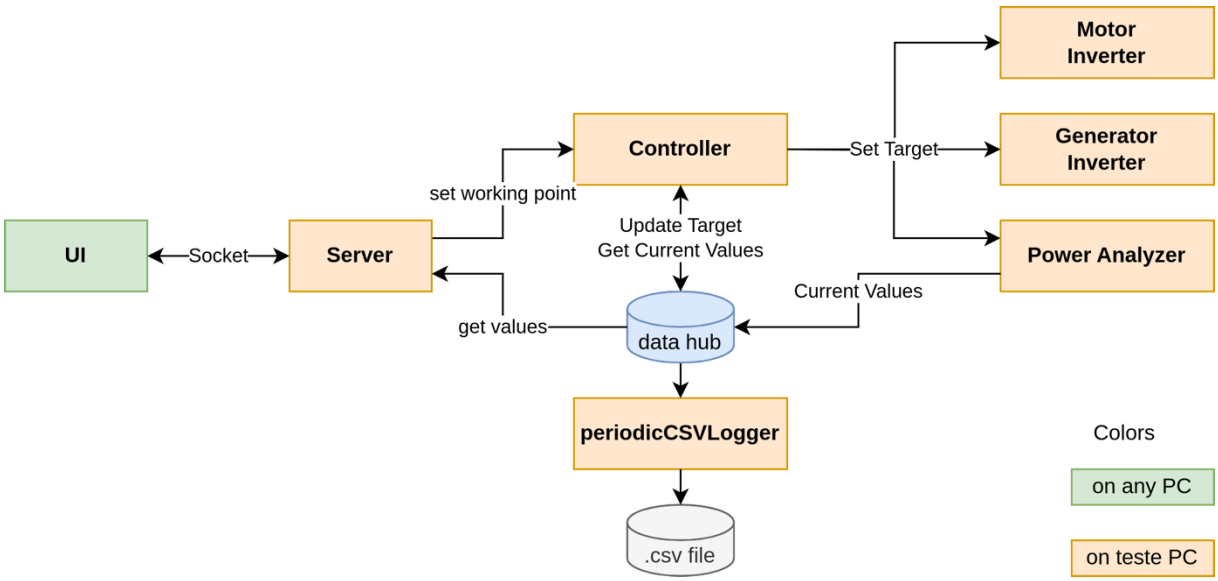


Figure 9: Software architecture of the test bench.

State machine

When freshly started, the system is in the ‘idle’ state, all inverters are switched off. If a new operating point is set (this is done via the server, see software architecture), the state changes to ‘Ramp Frequency’. In this state, the frequency is slowly ramped up until the target value is reached. It then switches to the ‘Control Torque’ state, in which the frequency of the load machine is regulated so that the desired torque is set. If a new operating point is now set, the machine returns to the ‘Ramp Frequency’ state and the cycle starts again (Figure 10).

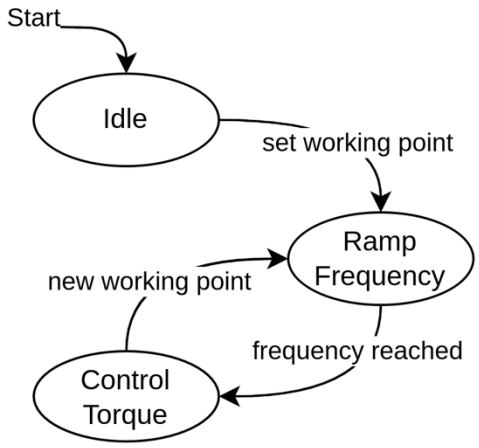


Figure 10: State diagram of the controller in the control software.

Basic characterisation of the Grundfos pump drive system

4.1 System boundaries for the efficiency measurements

The Grundfos reference system is characterised as a ‘Power Drive System’ (PDS) in accordance with IEC 61800-9. This means that the hydraulic part is removed from the motor shaft, as a PDS is defined from the mains connection to the motor shaft. In contrast, the system boundary of a ‘Complete Drive Module’ (CDM) is defined from the mains connection to the electrical connection point upstream of the motor.

According to Figure 11, the ‘Complete Drive Module’ in the reference system consists of the frequency inverter and the sine filter. Together with the pump motor, the components form the PDS, which is analysed in this project.

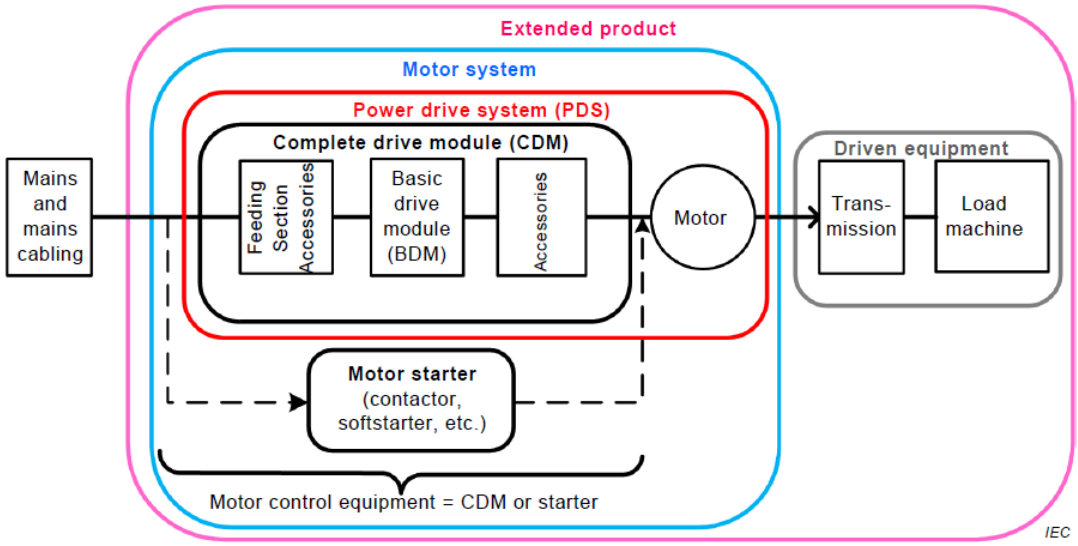


Figure 11: Extract from the IEC 61800-9-1 standard [8]. Illustration of the system boundary of a power drive system (red frame).

4.2 Frequency converter (CUE 3 x 380-500V IP20 5.5kW)

To better understand the structure, the components used and the function of the Grundfos frequency inverter, a second example was procured, dismantled and analysed. The main findings are summarised below.

Table 5: Extract from the manufacturer's data for the CUE 3 x 380-500V IP20 5.5kW frequency converter [5].

Parameter	Value
Motor nominal power P2	5.5 kW
Grid frequency	50 / 60 Hz
Nominal voltage	3 x 380-440/441-500 V
Nominal current	13-11 A
Maximum current from grid	13 A
Efficiency at rated power	97 %
Protection (acc. to IEC 34-5)	IP20
Ambient temperature	0 .. 50 °C
Relative air humidity	5 - 95 %
Installation	Wall mounting
Net weight	6.6 kg
Dimensions	130 x 268 x 205 mm

Key findings:

- A semiconductor module (manufacturer: Danfoss) is used, which contains both the diode rectifier and the IGBT-based inverter.
- The intermediate circuit is realised with two 680 µF electrolytic capacitors connected in series (total capacitance: 340 µF).
- A resistor is connected in parallel to each capacitor to ensure that the voltage per capacitor is not too high. Consequently, there are constant losses in the region of 5 W as soon as the capacitors are charged, even if no load is supplied.
- The frequency converter has an EMC line filter at the input and chokes integrated in the dc link to fulfil the standards for operation on the mains.
- The frequency converter is designed for a rated motor power at the shaft of 5.5 kW and must therefore be able to handle higher powers > 8 kVA.

Pictures of the disassembled frequency converter and its main components are shown in Figure 12.

Different control methods can be set for the operation of the motor on the frequency inverter. Voltage/frequency control is selected for the comparison between the commercial and the self-developed SiC frequency converter.

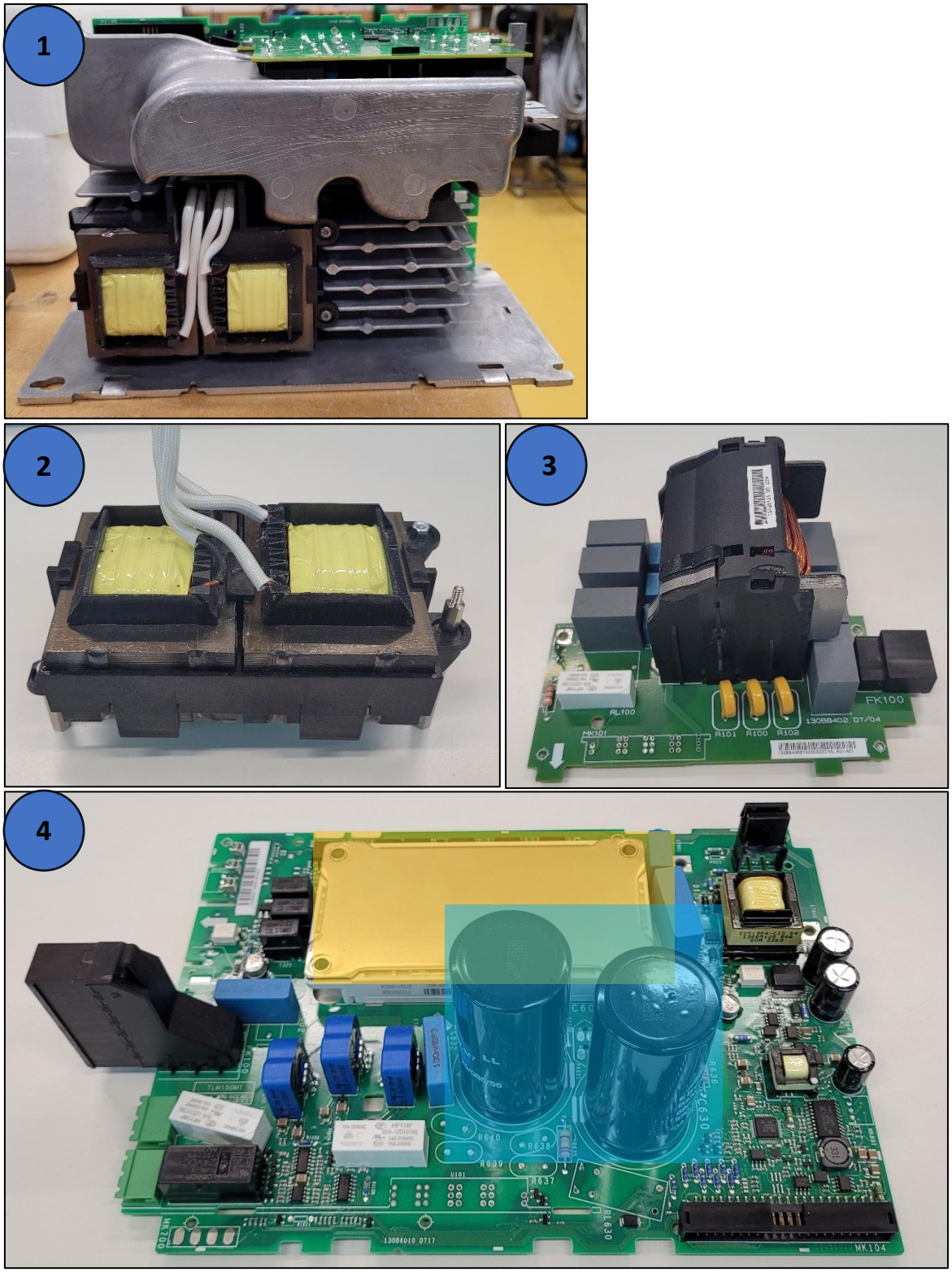


Figure 12: Photos of the assembled frequency converter without housing (1) and of its main components, DC link chokes (2), EMC line filter (3) and the main circuit board (4). On the picture of the main circuit board, the semiconductor module, consisting of rectifier and inverter, is highlighted in orange and the DC link capacitors in blue.

4.3 Output filter

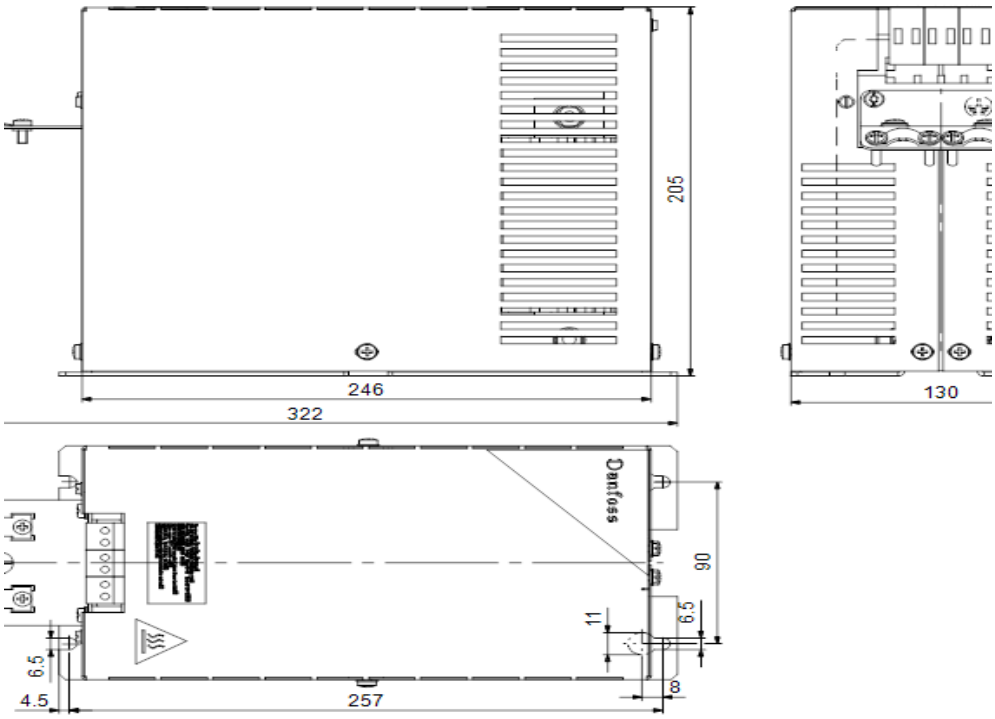


Figure 13: Dimensioned drawing of the sine filter (source: Grundfos [6]).

Table 6: Extract from the manufacturer's data for the sine filter [6].

Parameter	Value
Grid frequency	50 Hz
Nominal voltage	*200-500 V*
Nominal current	17 A
Rated current at 100 Hz	13 A
Protection (acc. to IEC 34-5)	IP20
Cable cross-section	4 mm^2
Inductor losses	125 W
Installation	Wall mounting
Net weight	9.1 kg
Dimensions	130 x 266 x 205 mm (without strain relief)
Inductance	3.1 mH
Capacity	10 µF

The output filter of the reference system consists of a three-phase coupled inductance and capacitance. Analysis of the filter yielded an inductance value of 3.1 mH (for the number of turns N = 113), whereby the material of the magnetic core of the reference system is not known. The iron sheet of type M165-35S was assumed for this purpose.

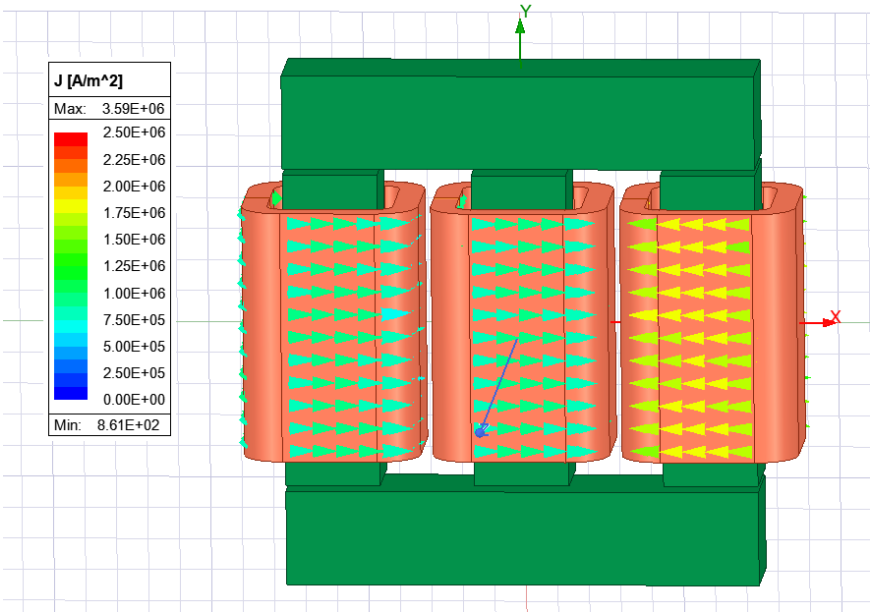


Figure 14: Simulation of the three-phase inductance in Ansys Maxwell. The windings (orange) are modelled as individual blocks, the arrows indicate the current direction, the relative amplitudes at the selected time are (-0.5, -0.5, 1). The magnetic core (green) consists of laminated iron sheets, with air gaps of 2 mm each at the transitions to the cross-connections.

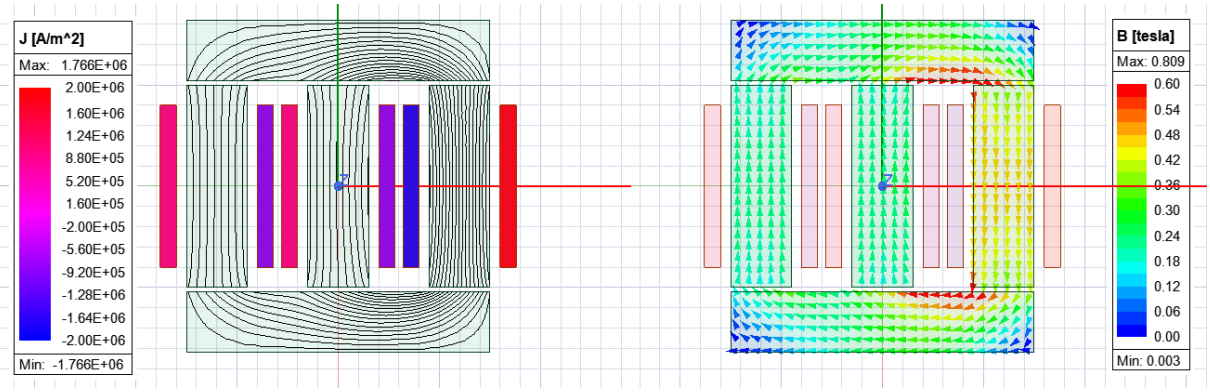


Figure 15: Left: The calculated flux lines through the magnetic core of the three-phase inductor are shown as lines, and the current density J in the windings is shown in colour (red=positive, out of the image plane, blue=negative, into the image plane). Right: The simulated magnetic flux density (B) is shown in colour and its direction is indicated by arrows.

The sine filter was characterised using a Bode 100 Network Analyzer from Omicron Lab:

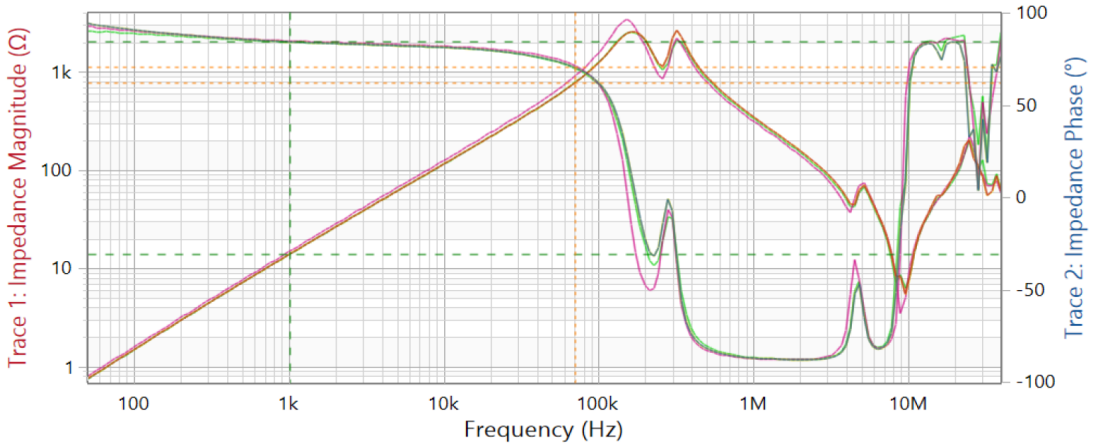


Figure 16: Measured frequency-dependent impedance (amplitude and phase) of the Grundfos filter inductances.

In summary, the analyses revealed the following trends with increasing frequency:

- Typically for an inductor, the impedance increases with increasing frequency from 50 Hz. Below 100 kHz, from approx. 10 kHz, the gradient changes visibly and then reaches resonance above 100 kHz. Further resonances occur at higher frequencies. The frequency behaviour then changes from inductive to capacitive, with the impedance decreasing again as the frequency increases.
- The behaviour of the filter impedance can also be seen in the phase. With inductive behaviour, the phase position is 90° and with capacitive behaviour -90°.
- At 50 Hz, the value of the individual filter inductance L_s is approx. 2.5 mH (3.1 mH is specified on the filter nameplate) and then decreases slightly. At 10 kHz, the value is already below 2 mH and shows a sharp drop above 100 kHz, after which the inductance becomes capacitive.
- At 50 Hz, the serial resistance R_s of the inductance is in the mΩ range but increases significantly at just a few kHz. At 10 kHz, the resistance is already approx. 15 Ω and at 70 kHz at 257 Ω.

The switch to SiC semiconductors, whose effects of which are being investigated as part of this project, opens up new possibilities in filter design. Increasing the switching frequency f_{SW} also allows the filter cut-off frequency f_c to be increased. This in turn depends on the value of the inductance:

$$f_c = 1/\left(2\pi\sqrt{LC}\right)$$

For example, a doubling off_{SW}, passed on as a doubling of f_c, leads to a four times smaller inductance L (with the same C). As a further degree of freedom, the inductance can be reduced by increasing the capacitance. With an electric motor, as a resistive inductive load, it is not advisable to increase the capacitance arbitrarily. There is a risk of exciting the resonance between the motor inductance and the filter capacitance.

Conclusion:

A minimum switching frequency of >5 kHz is required on the rating plate of the three-phase reference filter, but no maximum switching frequency is recommended. For the filter components of the reference filter, however, operation with switching frequencies >10 kHz is only advisable to a limited extent for energy-efficient operation. The cut-off frequency shifts with increasing frequency due to the changed values of the inductance and capacitance, so that the desired filter effect can no longer be guaranteed. The serial resistance of the filter coil increases significantly and thus also the losses at the higher

frequency components in the current. Obviously, however, these frequency components are strongly attenuated and hence do not cause higher losses in the increasing resistance value.

If the switching frequency exceeds 10 kHz, this filter should only be used with caution. In this case, a filter optimised for higher frequencies should be used, which has resonances clearly above the switching frequency.

4.4 MG132SC induction motor

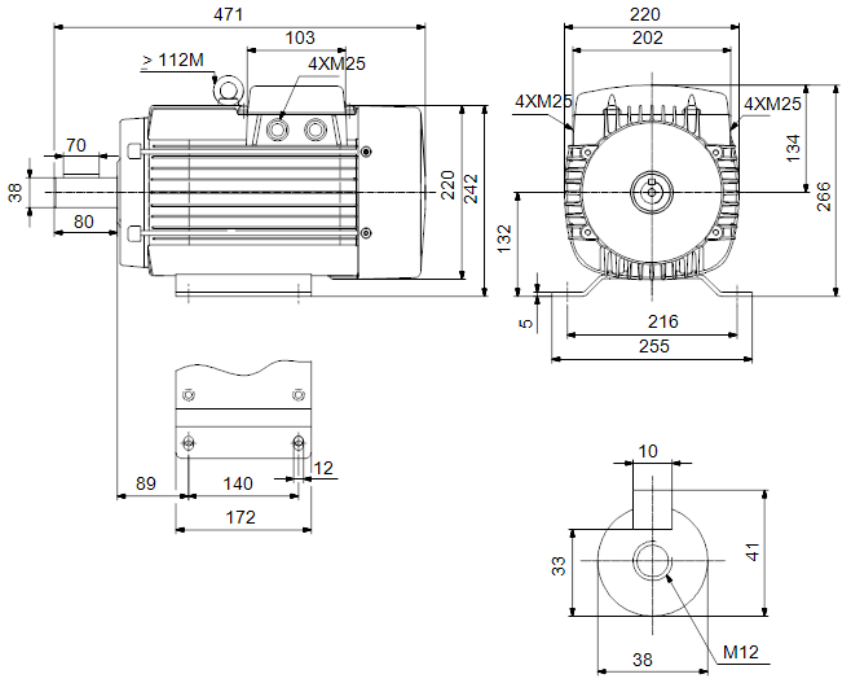


Figure 17: Dimensioned drawing of the pump motor manufacturer [7].

Table 7: Extract of the manufacturer data of the pump motor [7].

Parameter	Value
IE efficiency class	IE3
Nominal power P2	5.5 kW
Grid frequency	50 Hz
Nominal voltage	3 x 380-415D V
Nominal current	11 A
Max. current	12.2 A
Start-up current	1080-1180 %
Power factor Cos phi	0.87-0.82
Nominal speed	2920-2940 1/min
Nominal torque at full load	17.8 Nm
Starting torque	370-460 %
Tilting moment of the motor	460-550 %
Moment of inertia	0.0097 kg m²
Efficiency	IE3 89,2%
Efficiency at full load	89.2 %
Efficiency at ¾ load	90.0 %
Efficiency at ½ load	89.6 %
Magnetic poles	2
Ambient temperature	-30 .. 60 °C
Net weight	40 kg
Dimensions	255 x 266 x 471 mm
Mounting acc. to IEC 34-7	IM B3

The pump was disconnected from the motor. Couplings and devices have been procured to couple the pump motor to a load machine.

Development of the SiC converter prototype

5.1 Definition of requirements specifications

Using the components from Figure 12, it was possible to confirm that the inverter from Grundfos must be a standard frequency inverter as shown in Figure 18. Table 8 summarises the specifications of the developed SiC frequency converter.

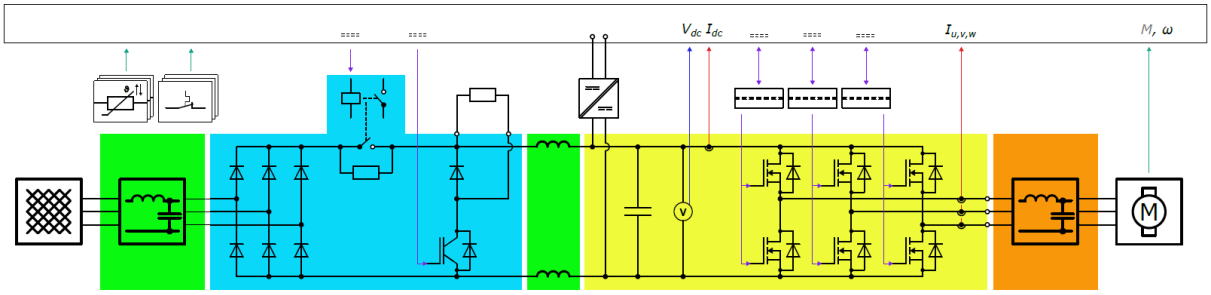


Figure 18: Block diagram of the circuit topology of the frequency converter.

Brief description of the SiC inverter:

- The power converter is designed for operation on a three-phase 400 V / 50 Hz mains supply.
- The mains supply the DC link capacitor (left in the yellow area in Figure 18) of the frequency converter via a B6U diode bridge (blue). The filters of the reference system (green) are re-used to comply with the current standards for operation on the mains supply. These consist of a three-phase filter on the mains and DC chokes in the positive and negative DC link paths. The components are shown in Figure 12 (photos 2 and 3).
- Pre-charging takes place via resistors when the DC link capacitor is not yet charged. A brake chopper circuit prevents the DC link voltage from being charged to a value that is too high for the components.
- On the load side, energy is drawn from the DC link via the drive inverter (yellow). The drive motor (far right) is brought to rotation. The speed follows the fundamental oscillation, which is generated by the PWM control of the inverter semiconductors.
- A sinusoidal filter (orange) is used between the inverter and motor to ensure that only sinusoidal voltages and currents drive the motor.
- The control board is shown as a block across all components of the power section just described in Figure 18. This is used to control the semiconductors, analyse measurements and provide protection by switching off when unauthorised conditions are detected.

Table 8 Specifications of the SiC-based frequency converter prototype.

Parameter	Value	Comment
Output power	8.5 kVA (P2 rated motor power: 5.5 kW)	110% overload capacity for 60 s every 300 s Pel: P2/89.2% x 110% = 6782 W Cos_phi = 0.87 - 0.82 S_motor_in = Pel/cos_phi = 8271 VA Ploss_filter = 150 W Sout_inverter > 8421 VA
Max. output current	25 A	For 8.5 kVA and normal (possibly also high overload with 160 %)
Input voltage diode rectifier	380 - 500 VAC (RMS Phase - Phase), 50 / 60 Hz	On 400 VAC mains
DC link voltage	Idle: 537 - 707 Vdc Under load: 513 - 675 Vdc	Corresponds to the rectified mains voltage
Cooling	Fan	Activation based on temperature measurement
Designed for	☒ High efficiency ☐ Reliability ☐ System costs ☐ Size / volume ☐ Weight ☐ Other	Standard switching topology Load profile-based analysis of energy savings Comparison with reference system
Ambient conditions	0 .. 50 °C 5 - 95 % ≤ 1000 m	Ambient temperature Relative humidity Installation altitude above sea level
Mechanical dimensions	Approx. 205 x 130 x 268 mm	External dimensions based on the reference design
Requirements	Use of SiC MOSFETs. Design should aim for energy savings for real operating cases. Design should be close to the industry standard	SFOE requirement
Purpose	☐ Functional model (proof of concept) ☒ Prototype for operation in the laboratory ☐ Towards series production	Conduct measurements in accordance with standard EN 61800
Extra	-	-

5.2 PLECS Simulation Model

The simulation model was realised with the PLECS software from Plexim GmbH. The individual system components are mapped in separate modules, which are linked to each other in the overall view. The individual components can therefore be developed and refined independently of each other. The overview diagram can be seen in Figure 19.

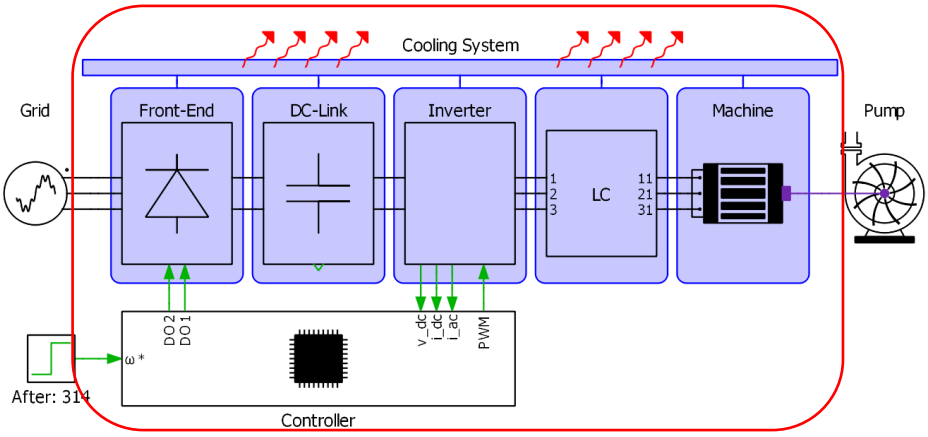


Figure 19: Block diagram of the generic simulation model of the pump drive. The system boundary of the PDS is marked with the red frame.

The subsystems of the model are:

- Grid: voltage source with 3 x 400 VAC / 50 Hz
- Front-end: Loss model of the B6 diode rectifier.
- DC link: Loss model of the DC link capacitors, as resistance (ESR) in series with the capacitance.
- Inverter: Model of the two-level frequency inverter. Semiconductors can be selected between IGBT or SiC-MOSFET (loss models for PLECS are provided by the semiconductor manufacturers)
- Filter: Model of a three-phase LC filter. Conventional electrical steel and the powder core material Kool-Mu can be selected as the core material. The losses are stored in a look-up table.
- Machine: Based on the motor data, the IEC 60034-31 [12] standard, in particular Annex A, is used to determine efficiency. IEC 60034-31 provides a loss calculation model which is used here to calculate the motor losses. Note that the loss model is valid only at fundamental frequency.
- Pump: The operating point (torque, speed) on the motor shaft is specified here.
- Cooling system: Thermal impedances are stored here, which describe the heat transfer from the respective heat source to the cooling medium or the ambient air.
- Controller: A voltage-frequency controller is implemented here to regulate the simulation. A constant value can be entered as losses. The losses of the controller used to operate the frequency converter were measured to around 20 W.

5.3 Selection of components

The frequency converter is made up of the parts marked in colour in Figure 18. The most important components in the power path can be determined according to the specifications in Table 8. The following points have been taken into account in the selection process to achieve an industry-orientated design:

- At least one other manufacturer should be able to supply the parts so that the layout does not have to be heavily customised (second source).
- If several components fulfil the technical requirements and promise better efficiency, they are selected according to criteria such as cost, availability, expandability, etc.
- Standardised semiconductor packages or modules should be used wherever possible. This simplifies the mechanical design.

AC-DC mains-side B6U rectifier with chopper configuration

On the mains side, the three-phase AC voltage is rectified by diodes to charge the DC link with direct current. Infineon offers a module for this purpose, which is available in the same housing as the module of the load-side power converter. The mechanical design can therefore be realised on one level or even on the same heat sink and the same circuit board.



Figure 20: Infineon DDB6U50N16W1R B6U rectifier module with chopper configuration. Image source: Infineon.

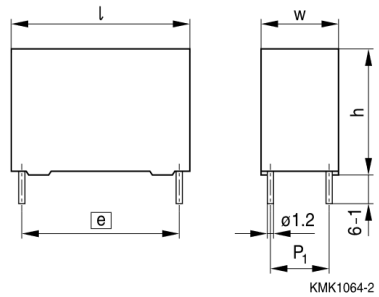
The selected diode module (Figure 20) uses silicon diodes rather than SiC diodes. It was selected because the expected losses during operation are lower than for SiC diode modules with comparable specifications.

DC link

DC link circuits are typically made with electrolytic capacitors. These are characterised by a high energy density, a low price but also higher losses. This is also how the intermediate circuit of the Grundfos frequency inverter was realised (Figure 12, Photo 4). The DC link of the reference system consists of two 680 µF electrolytic capacitors connected in series with balancing resistors in parallel to the capacitors (total capacitance: 340 µF).

The selected DC link capacitance for the SiC inverter is made up of six parallel 70 µF film capacitors totalling 420 µF. The choice of capacitance is based on the reference system and not on our own calculations, as the requirements of the converters to be compared are the same. The use of balancing resistors is not necessary, which eliminates the energy losses caused by balancing. At 900 V, the dielectric strength of the capacitors is sufficiently high in contrast to the 450 V of the electrolytic capacitors in the reference system. Figure 21 shows the selected capacitor type and its properties.

B32716H, B32718H



	B32716H	B32718H
Lead spacing e ±0.4:	37.5	52.5
Lead diameter d_1:	1.2	1.2

Dimensions in mm



C_R [1] µF	Max. dimensions w x h x l mm	P1 mm	Ordering code (composition see below)	$I_{RMS,max}$ 70 °C 10 kHz A	$I_{RMS,max}$ [2] 85 °C 10 kHz A	ESR_{typ} 85 °C 10 kHz mΩ	ESL_{typ} [3] nH	tan δ max 1 kHz 10^{-3}	tan δ max 10 kHz 10^{-3}	Pcs./ MOQ
$V_{R,85\ °C}$ = 900 V DC, $V_{op,100\ °C}$ = 720 V DC										
35.0	30.0x45.0x57.5	20.3	B32718H9356+000	18.2	15.8	5.8	14.5	2.3	22.7	280
45.0	35.0x50.0x57.5	20.3	B32718H9456+000	21.3	18.5	4.9	16.0	2.4	23.0	108
50.0	35.0x50.0x57.5	20.3	B32718H9506K000	22.7	19.7	4.3	16.5	2.4	23.0	108
55.0	38.0x57.5x57.5	20.3	B32718H9556+000	25.4	22.1	3.9	18.0	2.4	23.0	96
60.0	38.0x57.5x57.5	20.3	B32718H9606+000	26.5	23.0	3.6	18.5	2.4	23.1	96
65.0	45.0x55.0x57.5	20.3	B32718H9656+000	28.9	25.1	3.3	16.5	2.4	23.2	140
70.0	45.0x57.0x57.5	20.3	B32718H9706+000	30.7	26.7	3.0	17.5	2.4	23.2	140
85.0	45.0x65.0x57.5	20.3	B32718H9856K000	33.0	28.7	2.8	21.5	2.6	25.4	140

Figure 21: Data sheet extract TDK Metallized polypropylene Film Capacitor, Series/Type: B32718H.

The capacitor type fulfils the requirements and was chosen for the following reasons:

- very low inductance design (< 17.5 nH)
- low losses due to the ESR (3 mΩ).

Six of these capacitors are connected in parallel to achieve the desired total capacitance. This reduces the current per capacitor and thus further reduces the losses. The same applies to the parasitic inductance, which enables the SiC semiconductor to switch as quickly as possible with minimal losses.

DC-AC load-side power inverter

The load-side converter controls the motor. Pulse width modulation (PWM) is used to switch the SiC semiconductors via their gate drivers to supply the motor with the purest possible sinusoidal voltages and currents via the filter.

When selecting the semiconductors, attention must be paid to low switching energies, stray inductances and on-state resistances. SiC MOSFETs typically have significantly lower switching losses than silicon IGBTs of the same class. The conduction losses depend on the actual current. In general, SiC MOSFETs have advantages in the partial load range due to lower conduction losses compared to IGBTs, which catch up at higher currents. A significant reduction in losses is therefore expected for a typical pump application, which often operates in the partial load range.

SiC MOSFET semiconductor modules with a two-level three-phase full-bridge configuration in the 1200 V class are listed below with their main parameters. On-state resistance values <30 mΩ were favoured and therefore marked in green. Care was also taken to favour piece prices <200 CHF.

Table 9: Comparison of 1200 V SiC MOSFET modules in six-pack configuration (as of Nov. 2022).

Manufacturer	Type	On-state resistance [mΩ]	Price [CHF]	Availability / delivery time
Microchip Tech.	APTMC120TAM33 CTPAG	33	1'056	
Microchip Tech.	APTMC120TAM17 CTPAG	17	1'804	
Microchip Tech.	APTMC120TAM12 CTPAG	12	2'560	
Microchip Tech.	MSCSM120TAM31 CT3AG	31	401	
Microchip Tech.	MSCSM120TAM16 CTPAG	16	808	22
Wolfspeed	CCB021M12FM3	21	185	25
Wolfspeed	CCS050M12CM2	25	?	No longer recommended by the manufacturer for new designs
Semikron	SK40MD120CR03 ETE1	30-50	?	Sample Status
Infineon	FS05MR12A6MA1 B	5.5-9.1	1700	Mehrere Stück am IEE vorhanden inkl. Kühler
Infineon	FS45MR12W1M1_ B11	45	120	Several pieces available at the IEE incl. cooler
Rohm				

The selected module is the Wolfspeed CCB021M12FM3 (Figure 22: Wolfspeed CCB021M12FM3 six-pack SiC semiconductor module. Right: Wolfspeed half-bridge gate driver CGD1700HB2M-UNA. Image sources: Wolfspeed., left). It is available, has a comparatively low contact resistance R_{DSon} of 21 mΩ and yet a relatively favourable price. Other variants of this module are available with an R_{DSon} of 32 mΩ, but at a slightly lower price. The Infineon FS45MR12W1M1_B11 module follows with the same housing and pin assignment. It can be used as a second source for the favoured module from Wolfspeed. The Infineon module is 35 % cheaper. However, depending on the operating point, it has at least twice the R_{DSon} and therefore twice the conduction losses.



Figure 22: Wolfspeed CCB021M12FM3 six-pack SiC semiconductor module. Right: Wolfspeed half-bridge gate driver CGD1700HB2M-UNA. Image sources: Wolfspeed.

Further advantages are that ready-made half-bridge drivers are available for the SiC MOSFET modules (Figure 22). This allows the semiconductors to be controlled directly by a controller and switched safely and without interference with the necessary isolation and robustness. As described further above in this section, the diode rectifier module is also available in the same housing type or could be determined as such due to the choice of SiC MOSFET module.

Controller Hardware

The controller hardware is based on a previous project in which an H-bridge was realised to generate a single-phase AC voltage. The previous setup is being expanded and redesigned for the new 3-phase inverter. The advantage of building on the basis of the previous project is that large parts of the hardware have already been tested and their functionality and reliability have been verified.

The design of the electronics is based on a modular system in which the individual functions of the inverter are divided into different PCB levels. The individual levels are interconnected via electrical plug connections to distribute signals and the power supply to all levels. Figure 23 shows the block diagram.

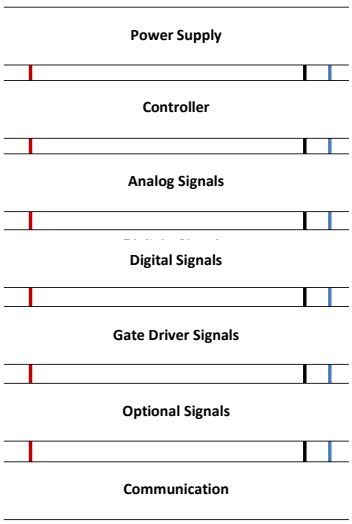




Figure 23: Left: Block diagram of the modular design of the electronics. Right: Photo of the developed controller hardware, consisting of several plug-in cards, according to the block diagram and a connection board (back-plane).

5.4 Mechanical Concept

The components described in section 5.3 were assembled into an inverter as shown in Figure 24. The frequency converter consists of two power boards: rectifier board (blue frame) and inverter board (yellow frame on the right). The EMC line filter and dc link chokes are highlighted in orange frames. The mains input and the connection for the sine filter at the output of the inverter are highlighted in purple.

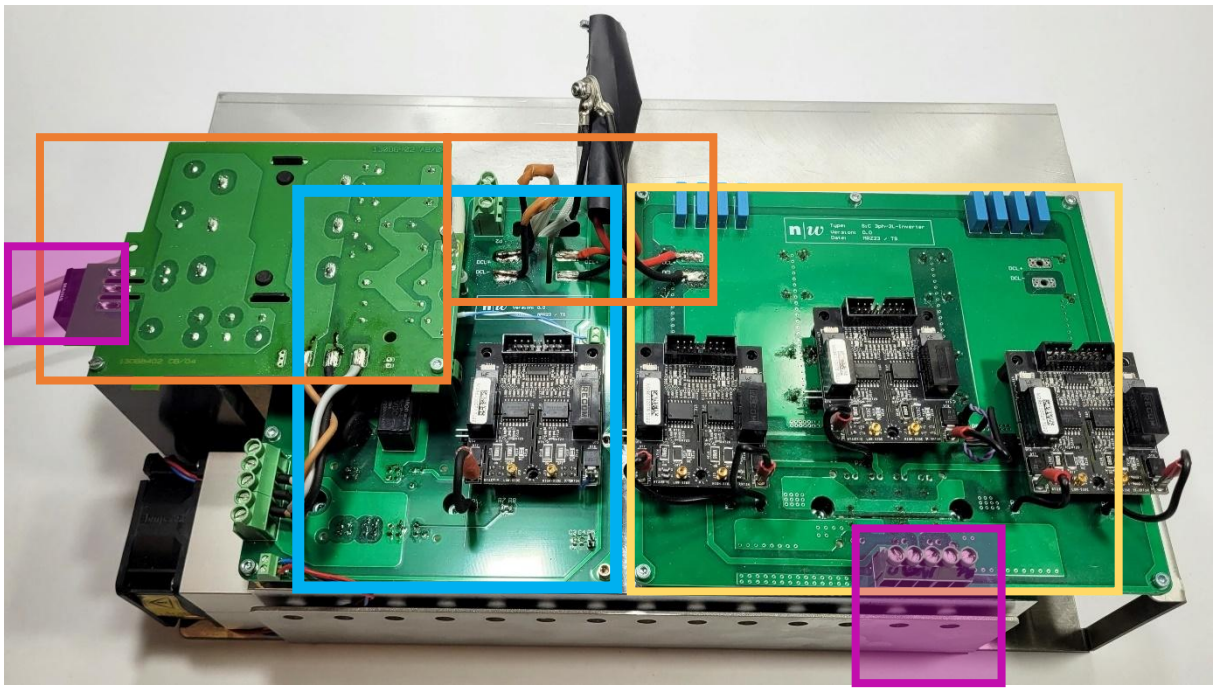


Figure 24: Top view of the mechanical structure of the SiC frequency converter; input grid filter (left), rectifier board (mid left), dc link and inverter board (right).

The semiconductor modules are attached to a heat sink (type: LA V6 from Fischer Elektronik), whereby the heat sink is ventilated with ambient air by a fan as soon as necessary. The DC link capacitors are soldered to the inverter board from the bottom side.

The gate drivers of the inverter modules are plugged into the inverter board from the top. The controller hardware is installed next to the power section. The signals are then exchanged between the controller and the power section via flat wire cables. In this way, the value of the temperature-dependent resistor integrated in the SiC semiconductor module is read out. Since it is located close to the semiconductor chips, a good approximation of the case temperature close to the chips (junction) during operation is possible.

Figure 25 and Figure 26 show more views of the SiC frequency converter.

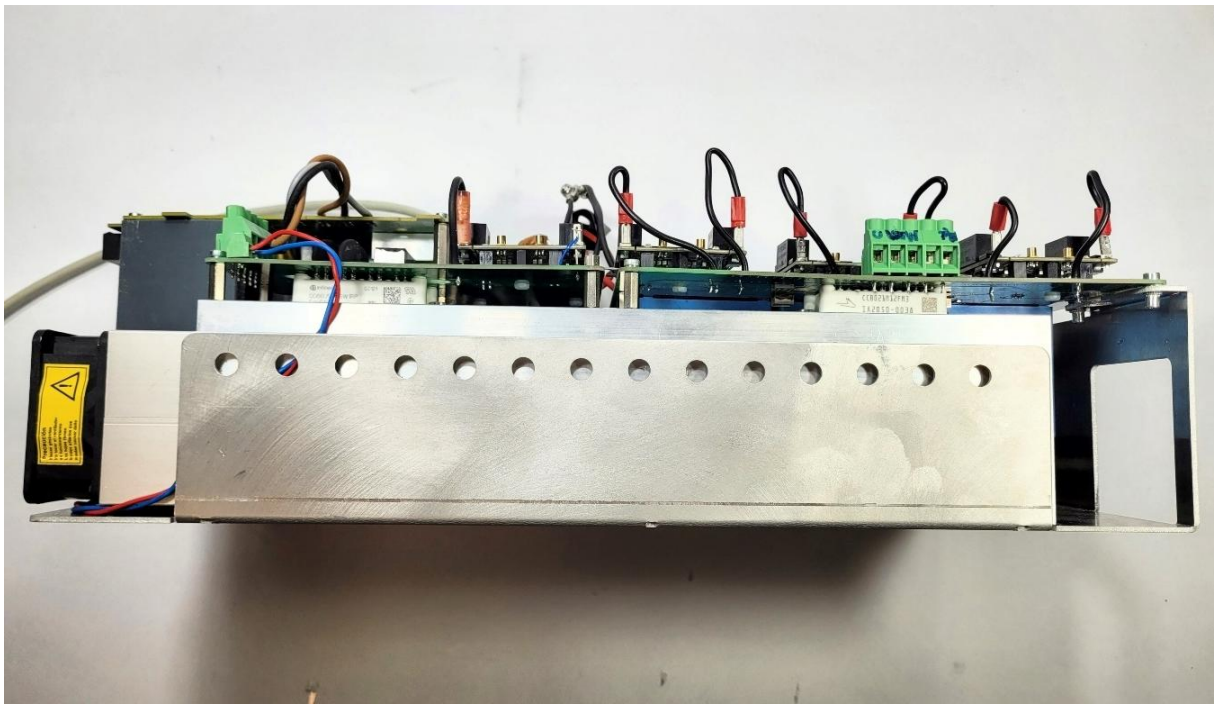


Figure 25: Side view of the SiC frequency converter; rectifier board with diode bridge module (left) mounted on the heatsink, dc link PCB with inverter module mounted on the heatsink (right).

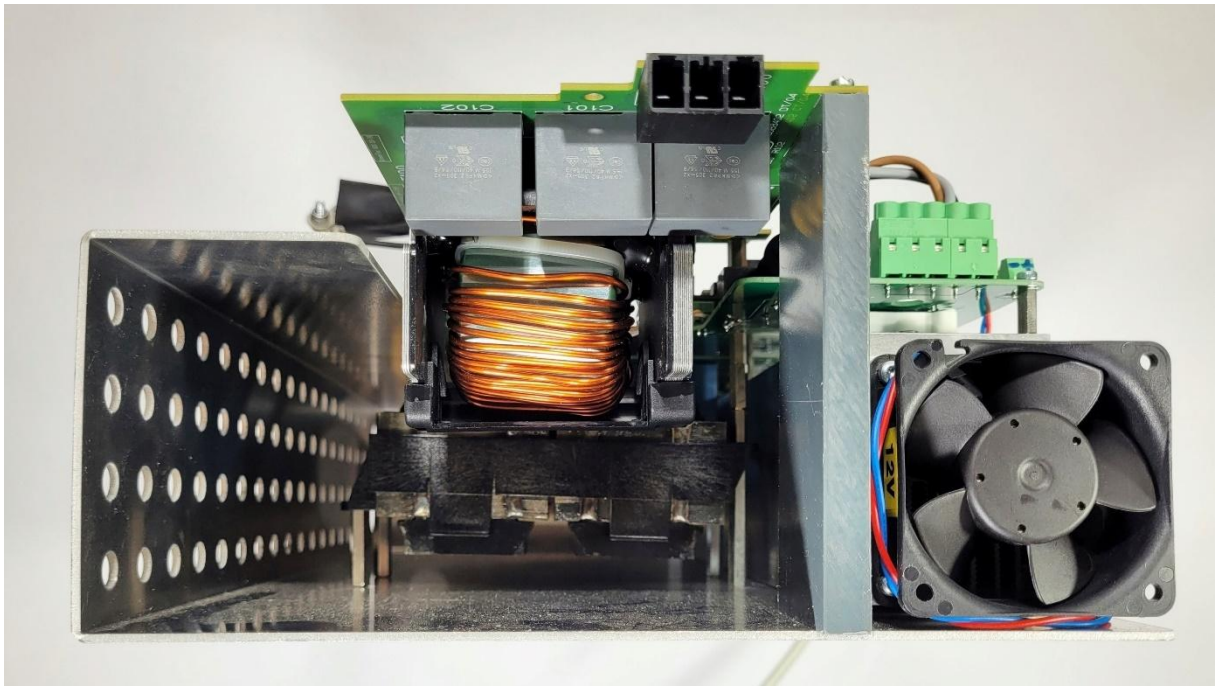


Figure 26: View of the SiC frequency converter from the mains input side; input grid filter from Grundfos frequency converter (top) and dc chokes (bottom), fan of the heatsink (right).

Development of the motor-side filter

A three-phase filter was developed as an alternative to the reference filter as part of a student bachelor's thesis [13] with the aim of increasing efficiency. A metal powder core was used for the inductance in this filter. This material (‘Kool-Mu’ [14]) is characterised by lower losses at high frequencies compared to standard electromagnetic steel sheets.

6.1 Influence of the current ripple on the losses

The influence of the current ripple resulting from the switching frequency of the inverter semiconductors was investigated by measurements. For this purpose, two single-phase LC sine filters with a cut-off frequency of 1 kHz and the same values for inductance and capacitance were made. One filter was constructed with an M165 sheet iron core and the second filter with the core material “Kool-Mu” [14]. In terms of quality, both filters show a significant decrease in total losses (copper and core losses) when the switching frequency is increased up to 30 kHz which corresponds to 30 times of the corner frequency (1 kHz), see Figure 27.

The measurements show that the residual ripple of the current flowing into the filter contributes significantly to the overall losses of the filter. The choice of core material also has a significant influence on the losses, with 40% fewer losses occurring in the filter with the Kool-Mu material than in the filter with a laminated core (Figure 27). Increasing the switching frequency therefore reduces the filter losses.

This trend is confirmed for the three-phase filter of the reference system. Increasing the switching frequency from 5 kHz to 9 kHz reduces the filter losses by at least 15% with a sinusoidal current of 17 ARMS and a fundamental frequency of 50 Hz (Figure 28).

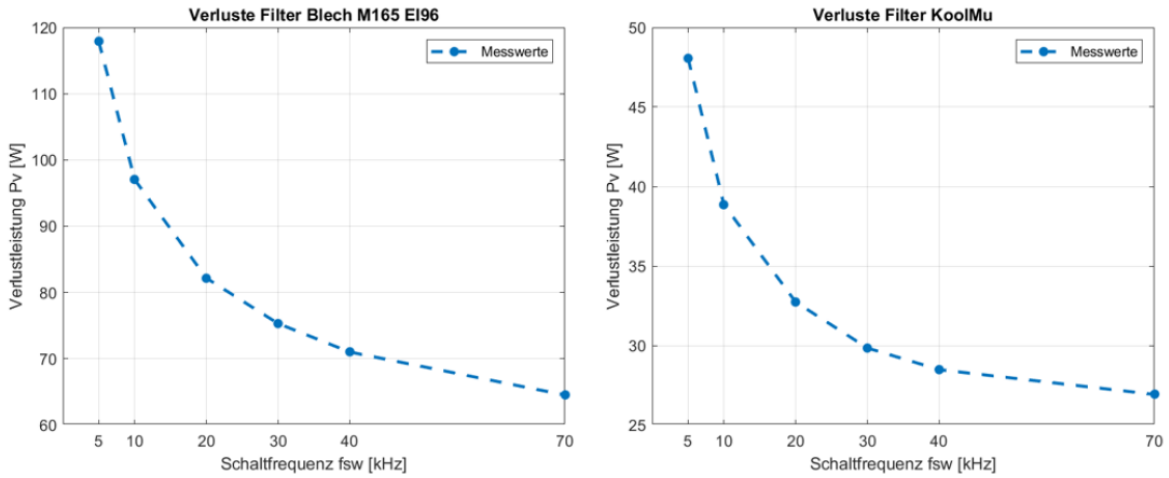


Figure 27: Power loss as a function of the switching frequency for single-phase filters with a sine-modulated current of 17 A and 50 Hz. Left: Core material M165; right: core material Kool-Mu. In both filters, losses decrease with increasing switching frequency. The losses of the Kool-Mu filter are less than half compared to the losses in the M165 filer over the entire tested frequency range.

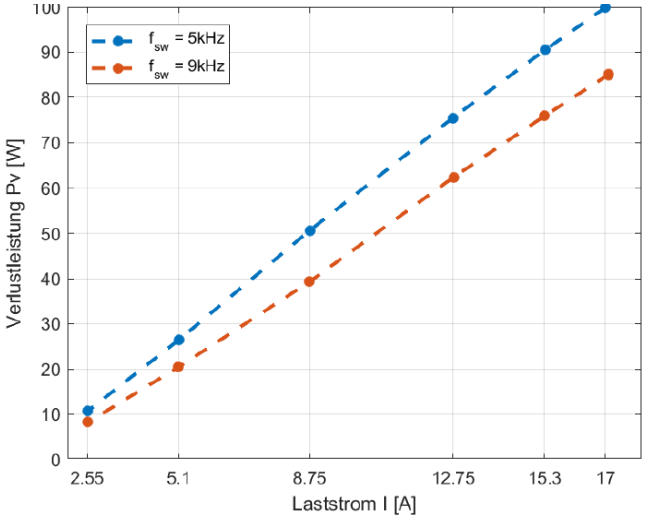


Figure 28: Measured power loss (P_v) of the filter manufactured by Grundfos (Danfoss) as a function of the current at a switching frequency of 5 kHz (blue) and 9 kHz (red).

The current ripple also causes losses in the motor. Reducing the current ripple is therefore important to reduce the losses of the entire drive system.

Boundary conditions and restrictions:

- The filter inductance causes significantly more losses than the filter capacity. It should therefore be kept as low as possible.
- To achieve a desired cut-off frequency of the filter, the filter inductance can be reduced if the filter capacitance is increased to the same extent.
- The filter capacitance must not be increased arbitrarily, as otherwise stable operation of the motor can no longer be guaranteed. The resonant circuit, consisting of filter capacitance and motor inductance, is not damped, especially when idling, and should therefore not be excited by the frequencies of the inverter.
- The magnetic core material and the geometry for the three-phase filter are determined based on the following parameters:
    - Material for which the lowest possible core losses are to be expected.
    - Availability
    - The maximum size of the filter should be within the range of the reference filter.

The switching frequency should be at least 10 times the cut-off frequency of the filter to dampen the current ripple sufficiently. Typical current curves are shown in

Figure 29.

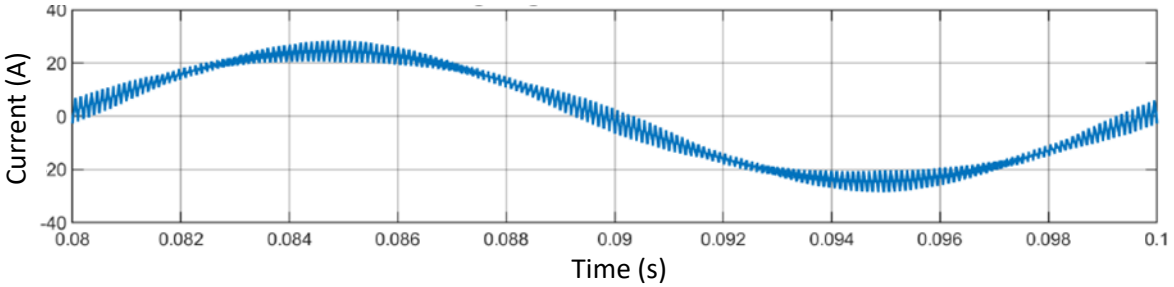


Figure 29: Simulated filter inductance current, which is made up of a 50 Hz and higher frequency components caused by the 10 kHz switching frequency of the inverter.

With the boundary conditions and restrictions described above, one of several low-loss designs was selected. The optimum design is marked with a red arrow in Figure 30 and has the values L = 780 µH and C = 30 µF. This results in the cut-off frequency f_c = 1,000 Hz. The selected factor f_sw /f_c = 10 results in a switching frequency of f_sw = 10 kHz. With this design, around 104 W losses are expected in the sine filter and the power converter together.

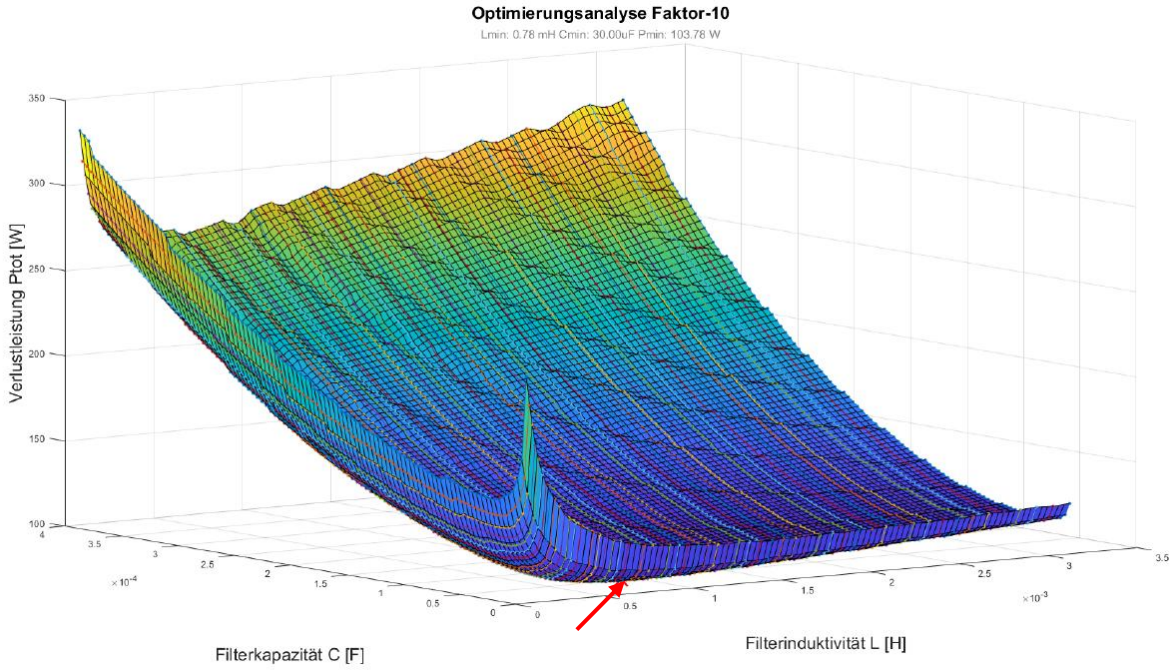


Figure 30: Optimisation results for an inverter and sine filter design. The X and Y axes span the area that determines the cut-off frequency of the LC-filter filter of second order, consisting of an inductance and a capacitance. The Z-axis shows the total expected losses in the semiconductors and the filter. The solution that promises the lowest possible total losses is marked in red.

Figure 31 shows the sine filter developed according to the optimal values.

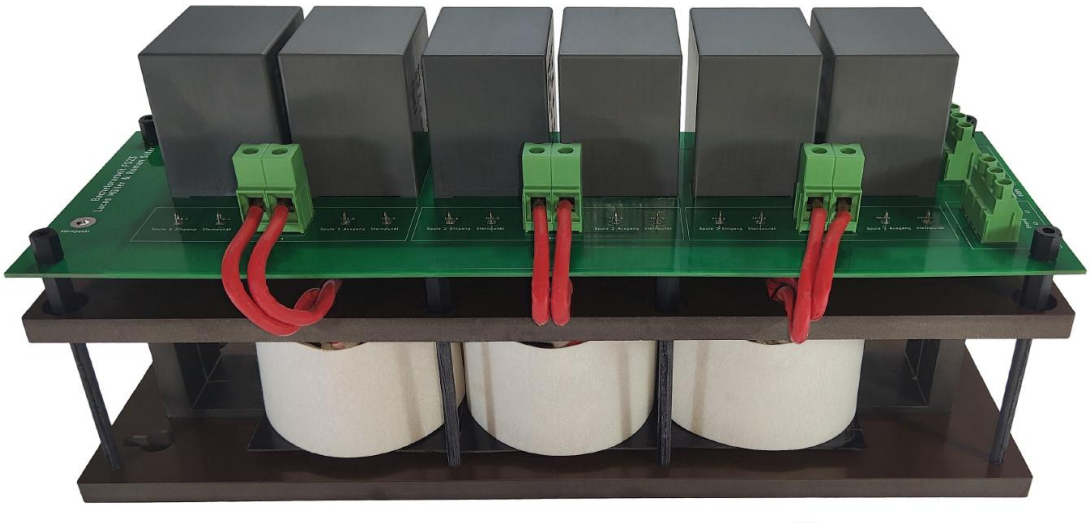


Figure 31: Photo of the three-phase motor filter with Kool-Mu core material. Above, two capacitors per phase. Three windings are visible at the bottom, which largely conceal the magnetic core.

The electrical data of the sine filter are given in Table 10.

Table 10: Type plate for the self-developed sine filter.

Parameter	Value
Grid frequency	50 Hz
Rated voltage	200-500 V
Rated current	17 A
Rated current at 100 Hz	13 A
Protection class (according to IEC 34-5)	IP00
Cable cross-section	4 mm2
Inductor loss	60 W (at 17 A)
Installation	wall
Net weight	9.1 kg
Dimensions	120 x 363 x 158 mm (without strain relief)
Inductance	780 µH
Capacitance	30 µF
Cut-off frequency filter	1’000 Hz
Switching frequency range	5 kHz - 20 kHz

Discussion and findings:

The optimisation algorithm finds its optimum solution at the cut-off frequency (1,000 Hz) of the filter, which is in the range of the cut-off frequency of the reference filter (900 Hz). This makes a direct comparison of the two filters possible.

It also shows that the switching frequency does not have to be increased to such an extent that frequency ranges are reached in which the natural resonances of the components are excited (see Figure 16). Even with the self-developed filter, the components showed natural resonances during the measurements with the Bode 100 measuring device. These are in the range of 150 kHz for the inductance and 40 kHz for the capacitance, consisting of two capacitors connected in parallel

6.2 Initial tests of the filter

First tests of the self-developed filter were carried out with a resistive load. In the application, the load is an asynchronous machine, which can have a different effect on the behaviour of the filter (due to its inductance, among other aspects) than the resistive load used here. See Chapter 0 for the efficiency measurements of the drive system.

Figure 32 shows the efficiencies of the reference filter and the Kool-Mu filter at switching frequencies around 9-10 kHz, as a function of the filter output power. The considerably higher efficiency of the Kool-Mu filter is clearly evident. At every operating point measured, the power loss was more than halved. The maximum measured efficiency was 99.6 % at 9 kW.

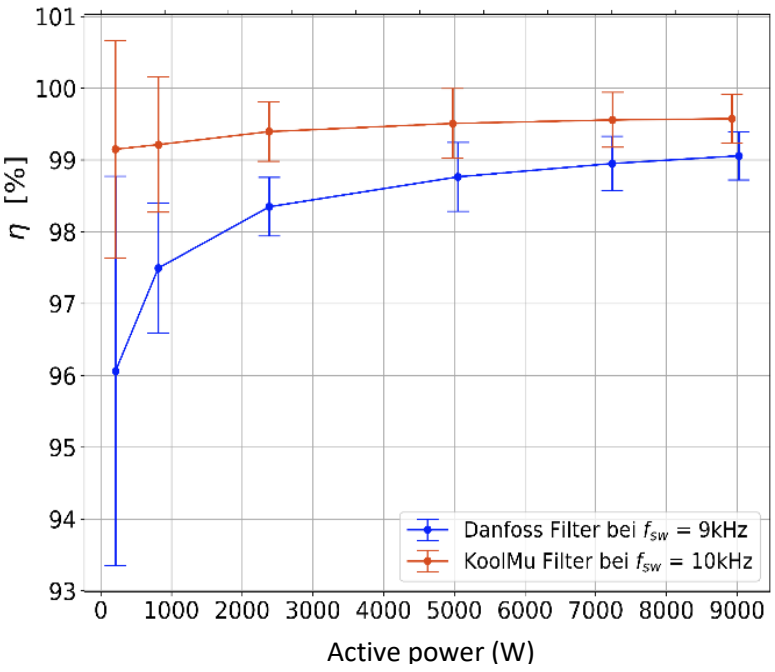


Figure 32: Measured efficiencies of the reference filter (blue) and the Kool-Mu filter developed here (red) as a function of the output power (resistive load). Measuring device used: HIOKI PW8001 Power Analyser [10].

Efficiency and loss measurements

7.1 Measurement setup

All measurements to characterize losses and efficiencies of each PDS were carried out in accordance with IEC 61800-9 with the test bench described in chapter 3.

The setup to connect the devices and to measure is the same for all configurations. A shielded motor cable of 10 m length is used with connected shielding to the frequency converter case, filter case and motor case.

Configurations:	SiC-FC or Grundfos-FC – Grundfos sine filter or FHNW sine filter – Grundfos motor
Control:	V/f control (for both SiC FC and Grundfos-FC)
Inverter switching frequency:	8 kHz up to 40 kHz
Power analyser mode:	50/60Hz
Power analyser sync-source:	First channel of measurement
Power analyser 3ph-wiring:	3P3W3M with Δ-Y conversion setting, since motor is in Δ-connection
Power analyser current sensor:	Phase compensation ON (Auto)

7.2 Measurement procedure

The measured data of the power analyser is stored as described in chapter 3.2. To evaluate the uncertainty of each operation point of the PDS, the following procedure has been applied:

The data points taken over the course of the measurement window at a defined operation point are cleaned. The data cleaning cuts of data at the beginning and at the end of a measurement time window and checks for data points exceptionally high or low.

The data cleaning must be applied since the power analyser stores the measured data continuously while the operation point changes during a measurement campaign. This is shown exemplary in Figure 33 (right), where the new operation point is approached, after the measurement time window of the previous operation point (left) has expired.

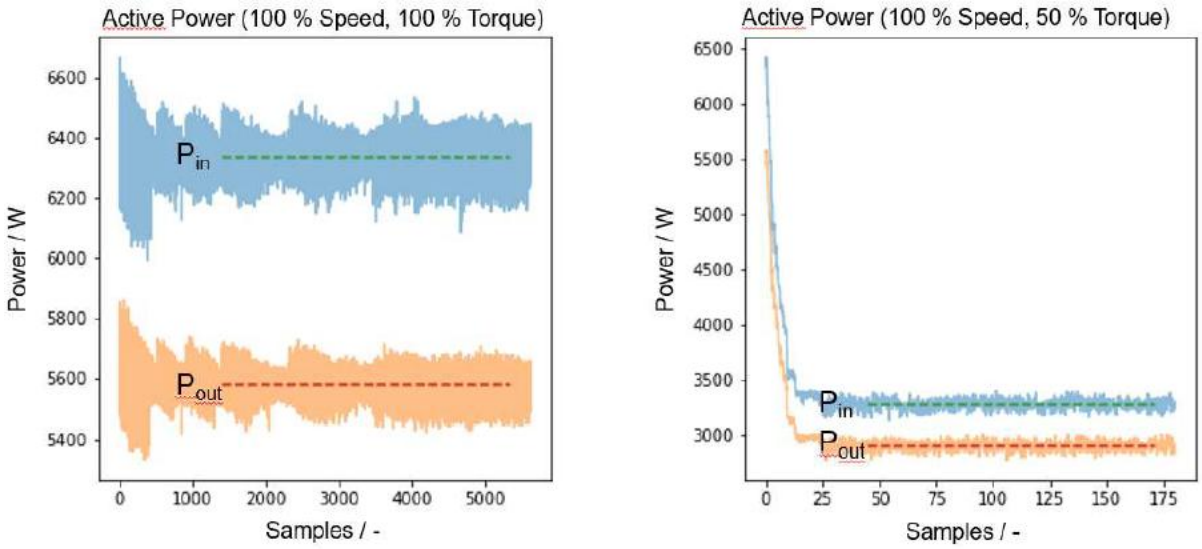


Figure 33: Measured input and output power data points of a PDS over the course of a measurement window. (left) At nominal power; (right) at nominal speed and 50 % of the nominal torque.

7.3 Measurement uncertainties

With the clean data, mean value, standard deviation and statistical uncertainty of the electrical power are calculated, furthermore the shaft speed and the torque. Using the actual measurement ranges, the device errors of reading and range are evaluated for each measurement at each operation point to calculate the systematic uncertainty. Note that the maximum guaranty errors are used and no assumptions were applied regarding the distribution between measurement intervals.

$$\Delta MG = (x\%\ of\ Reading) \cdot mean\ value\ of\ Reading + (y\%\ of\ Range)$$

The following table shows the accuracies applied for each measurement:

Electrical input power	% of Reading	% of Range
Current sensor CT6872	*0.03 %*	*0.007 %*
Power analyser PW8001	*0.01 %*	*0.02 %*
Active power measurement ($MPel$)	0.04 %	0.027 %

Speed sensor	% of Reading	Fixed Value
Speed sensor	0.01 %	0.5 / 360

Torque sensor	% of Reading	% of Range
Torque input of power analyser (MPA)	0.03 %	0.03 %
Torque sensor ($Msens$)	0	0.1 %

Combined uncertainty of torque measurement:

$$\Delta Mtq = \sqrt{\Delta MPA^2 + \Delta Msens^2}$$

Combining systematic and statistical uncertainty by the formula below gives the total uncertainty of each measurement.

$$\Delta Mtot = \sqrt{\Delta Msys^2 + \Delta Mstat^2}$$

The uncertainties of the PDS losses and the efficiencies at each operation point are calculated by error propagation.

$$\Delta \mathrm{M} = \sqrt{(\frac{\partial \mathrm{M}}{\partial \mathrm{x1}})^2 \cdot \Delta \mathrm{x1}^2 + \left(\frac{\partial \mathrm{M}}{\partial \mathrm{x2}}\right)^2 \cdot \Delta \mathrm{x2}^2 + \cdots + (\frac{\partial \mathrm{M}}{\partial \mathrm{xN}})^2 \cdot \Delta \mathrm{xN}^2}$$

With

$M1 = \eta = \frac{Pmech}{Pel}$	For the uncertainty of the efficiency
$M2 = Ploss = Pel - Pmech$	For the uncertainty of the power losses

7.4 Grundfos variable speed drive with commercial filter

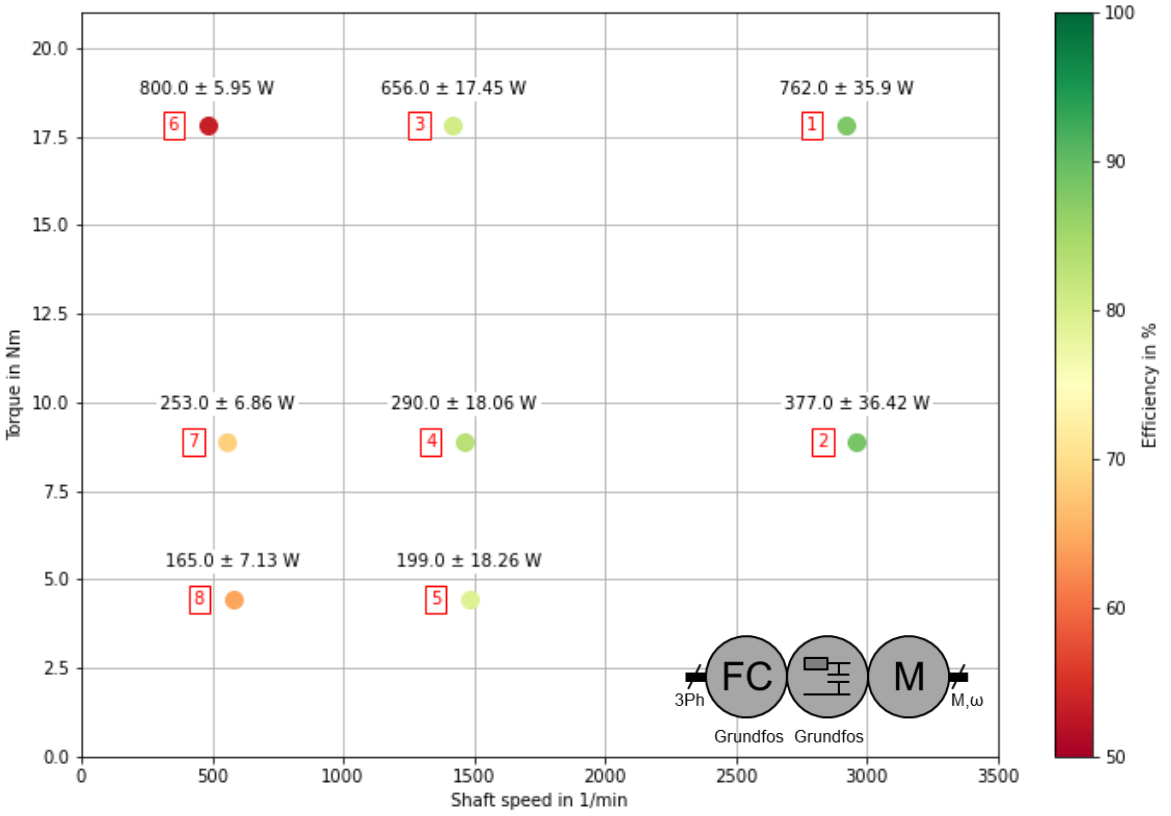


Figure 34: Loss map according to IEC-61800-9-2 of the PDS with a frequency converter of Grundfos (inverter switched at 8 kHz), the Grundfos sine-wave filter Grundfos and the pump motor. The coloured dots are the measured power losses per operation points where the colour corresponds to the efficiency of the system according to the bar on the right.

7.5 SiC variable speed drive with commercial filter

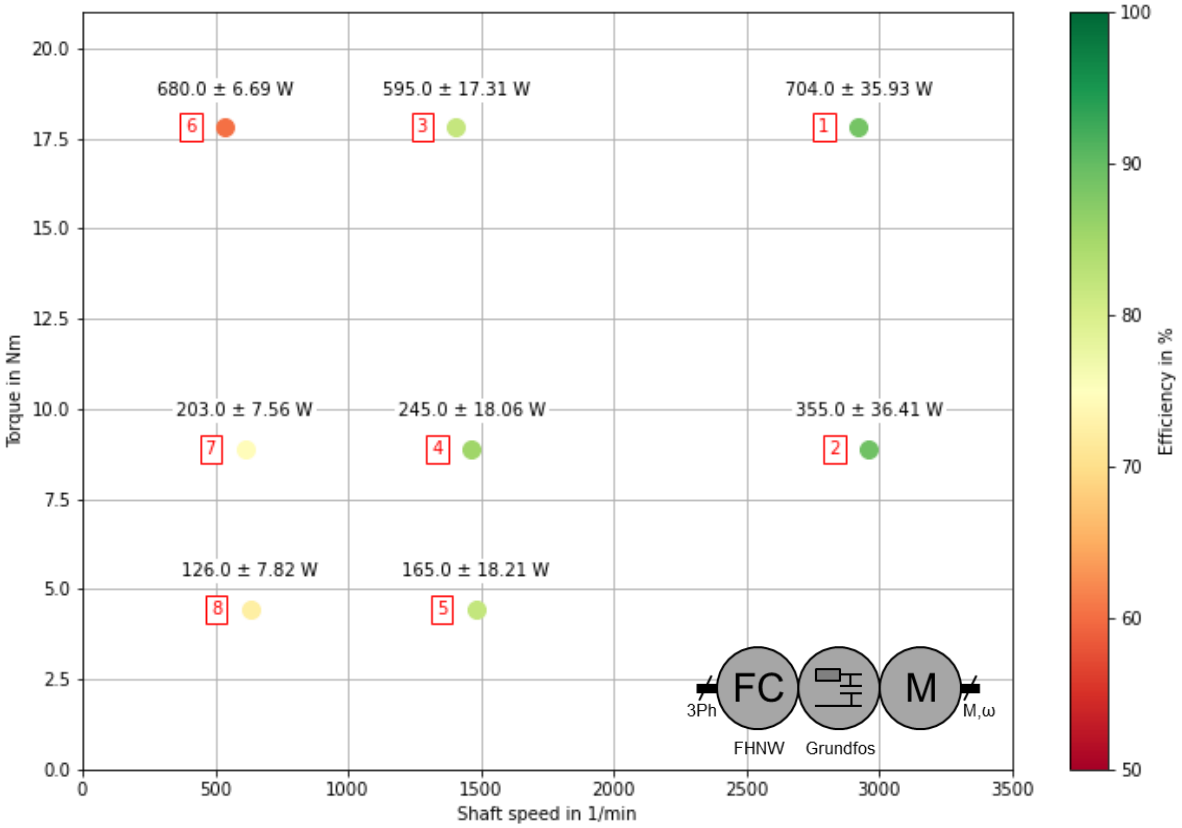


Figure 35: Loss map according to IEC-61800-9-2 of the PDS with the frequency converter developed by FHNW (inverter switched at 8 kHz), the Grundfos sine-wave filter and the Grundfos pump motor. The coloured dots are the measured power losses per operation points where the colour corresponds to the efficiency of the system according to the bar on the right.

7.6 SiC variable speed drive with Kool-Mu filter

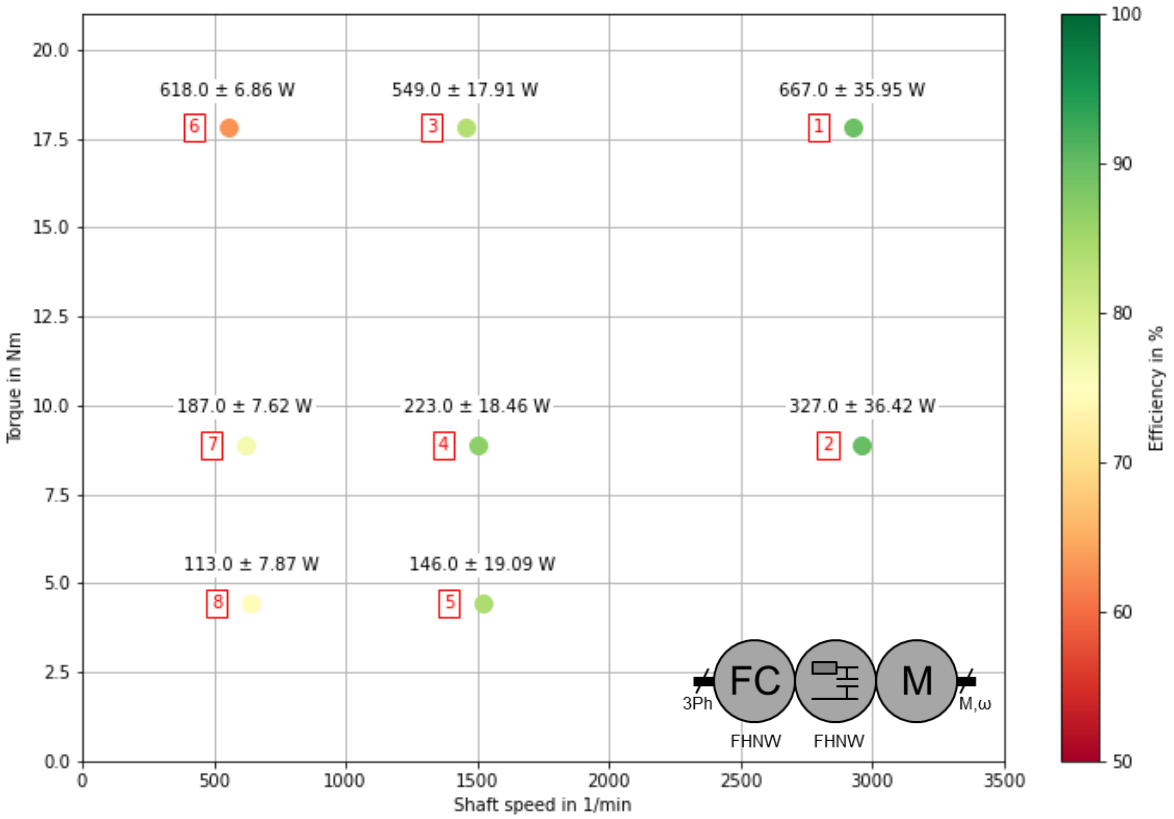


Figure 36: Loss map according to IEC-61800-9-2 of the PDS with the frequency converter developed by FHNW (SiC inverter switched at 8 kHz frequency), the sine-wave filter of FHNW with Kool-Mu core material and the Grundfos pump motor. The coloured dots are the measured power losses per operation points where the colour corresponds to the efficiency of the system according to the bar on the right.

Conclusions from the measurements

8.1 Efficiency comparison

The PDS loss maps displayed in Chapter 0 can be displayed as efficiency map in a contour plot.

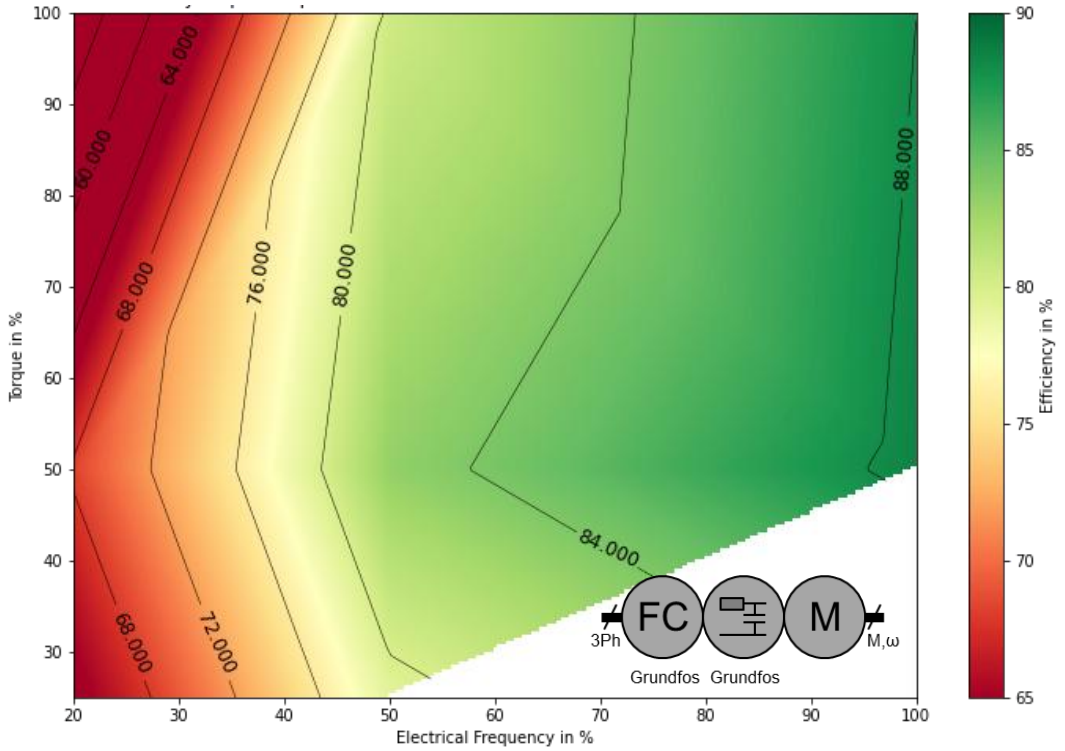


Figure 37: Contour plot for efficiency for PDS with Grundfos frequency converter, switched at 8 kHz and Grundfos sine filter.

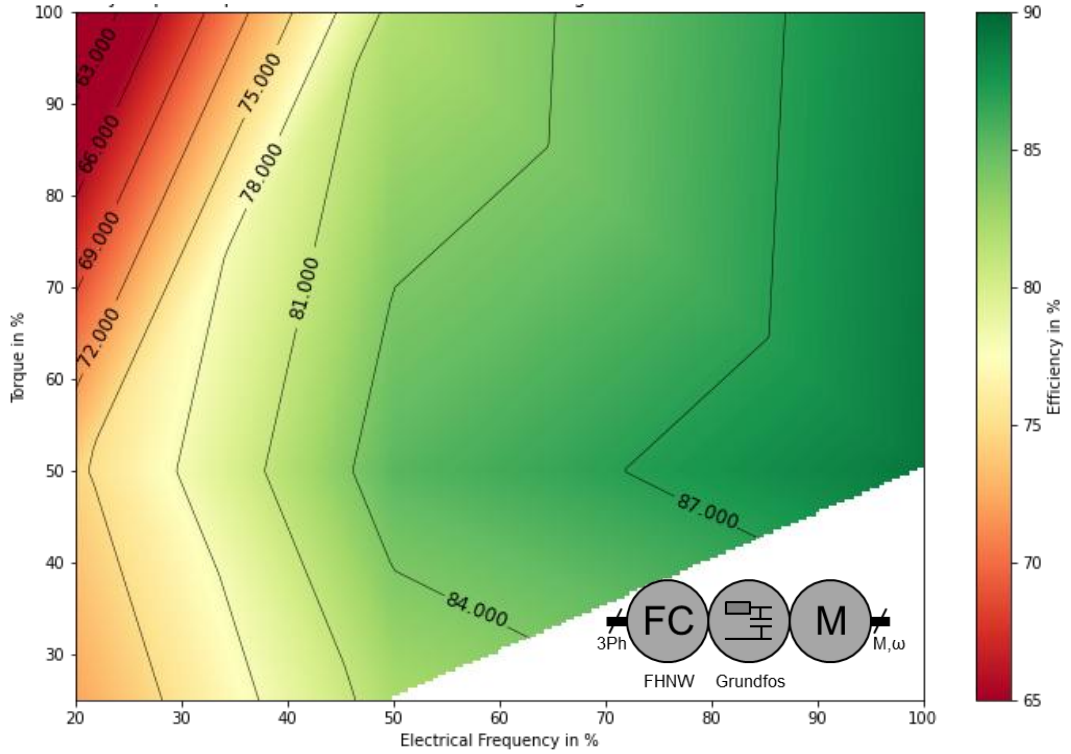


Figure 38: Contour plot for efficiency for PDS with SiC frequency converter, switched at 8 kHz and Grundfos sine filter.

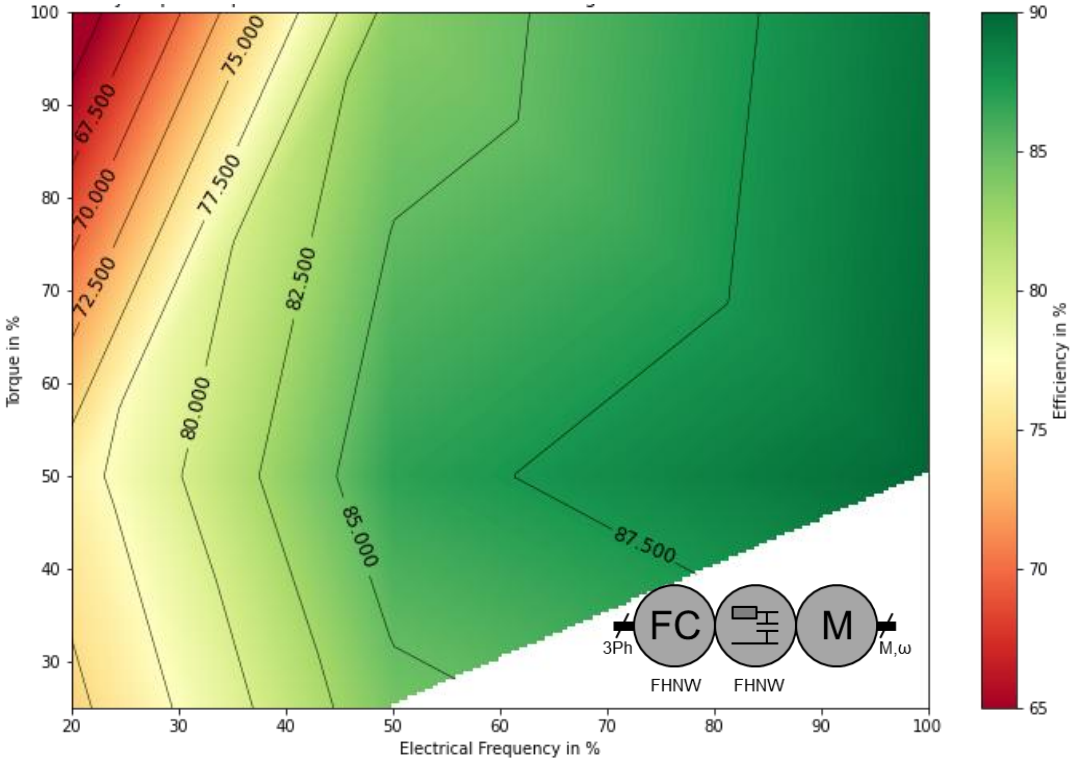


Figure 39: Contour plot for efficiency for PDS with SiC frequency converter, switched at 8 kHz and sine filter with Kool-Mu core material.

From the contour plots above one can see that changing from the IGBT-based inverter (Grundfos) to the inverter using SiC MOSFETs (FHNW) pushes the less efficient red areas below 70 % efficiency to lower shaft speed and high torque regions solely. Before, the efficiency was below 70 % even for low torque. The 68 % efficiency line in Figure 37 is lifted by 4% to 72 % in Figure 38. Consequently, the green high- efficiency area above 80 % increases more into the lower partial-load regions.

Changing the sine filter from Grundfos with one using a Kool-Mu core material brings additional improvements in efficiency and expansion of the green area, as depicted in Figure 39.

In the following chapter, losses are investigated when increasing the switching frequency.

8.2 Impact of the switching frequency on SiC PDS losses

In the previous sections, the losses and efficiencies were determined when exchanging components of the PDS. Here, the effect of the SiC inverter's switching frequency on the total PDS losses is investigated. The question is, if the losses caused by the current ripple in the filter and motor decrease more than the additional switching losses rise.

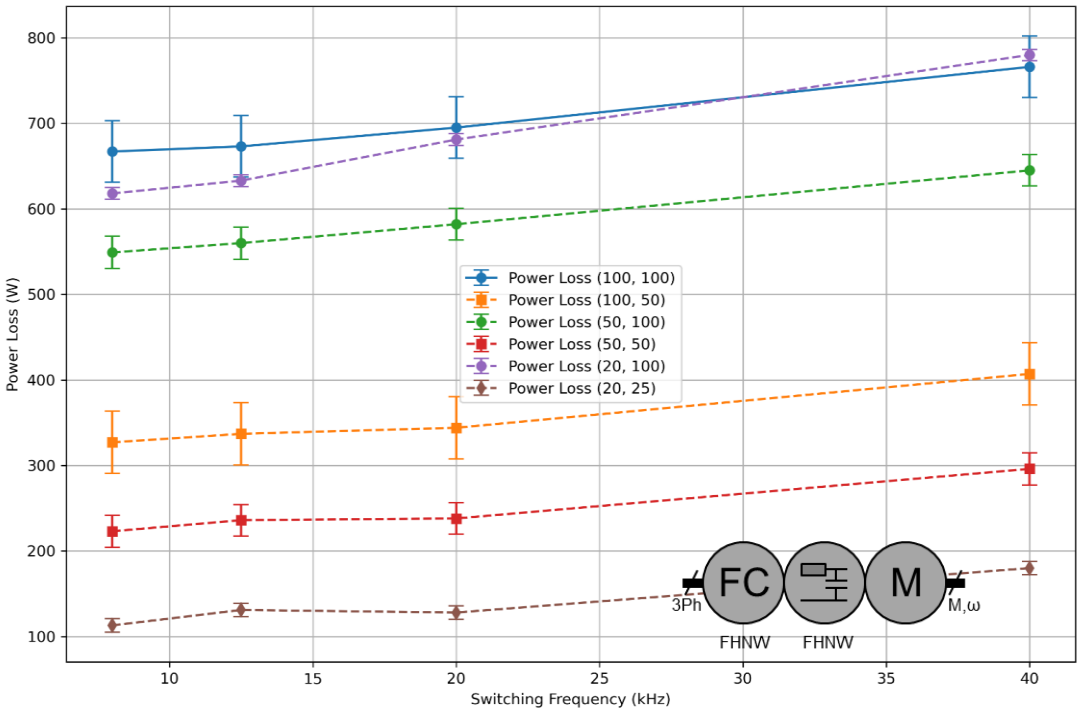


Figure 40: (Coloured lines) Evolution of power losses with rising inverter switching frequency of the PDS (SiC frequency converter and sine filter with Kool-Mu core material) at different operation points.

Finding:

Increasing the switching frequency does not reduce the total losses - they increase.

By adding a power measurement at the frequency converter output, the PDS losses can be separated into the losses of the frequency converter and the combined filter and motor losses. It must be mentioned that the measurement adds an uncertainty, but it shows the effects and trend of the loss evolution with rising inverter switching frequency. The accuracy of the total PDS losses measurement stays valid. Therefore, the uncertainty of this intermediate measurement can be split and assigned to the losses of the converter and the filter and motor losses.

In the following figures, the energy consumption of the frequency converter controller with measurements is measured separately and stays at 20 W to 21 W. The losses of the SiC semiconductors of the

inverter are simulated using the thermal loss model of the manufacturer. Hence, the remaining losses for grid filter, diode rectifier and dc link are calculated from the measured power losses minus the by simulation estimated inverter losses.

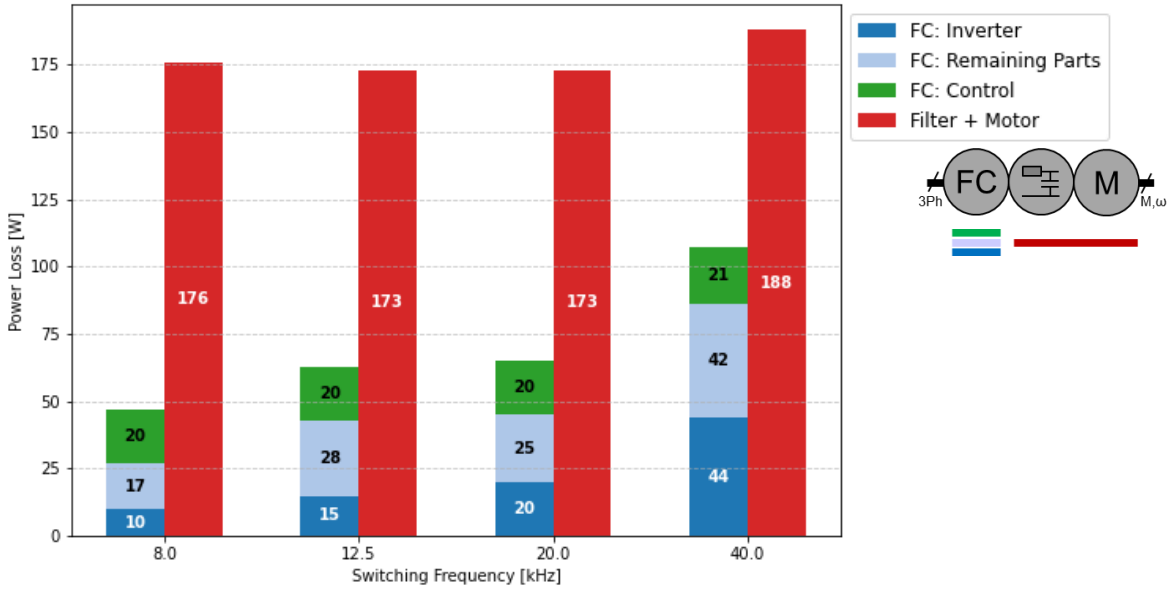


Figure 41: Breakdown of PDS power losses and their evolution with the switching frequency of the inverter. The distribution into the partial losses is based on the measurement of the total PDS losses and simulated and calculated part losses, where the uncertainty is unknown and therefore not shown. In addition, this uncertainty could not be assigned to either the converter or the filter and motor losses.
Operation point: 50 % of nominal shaft speed, 50 % of nominal shaft torque.

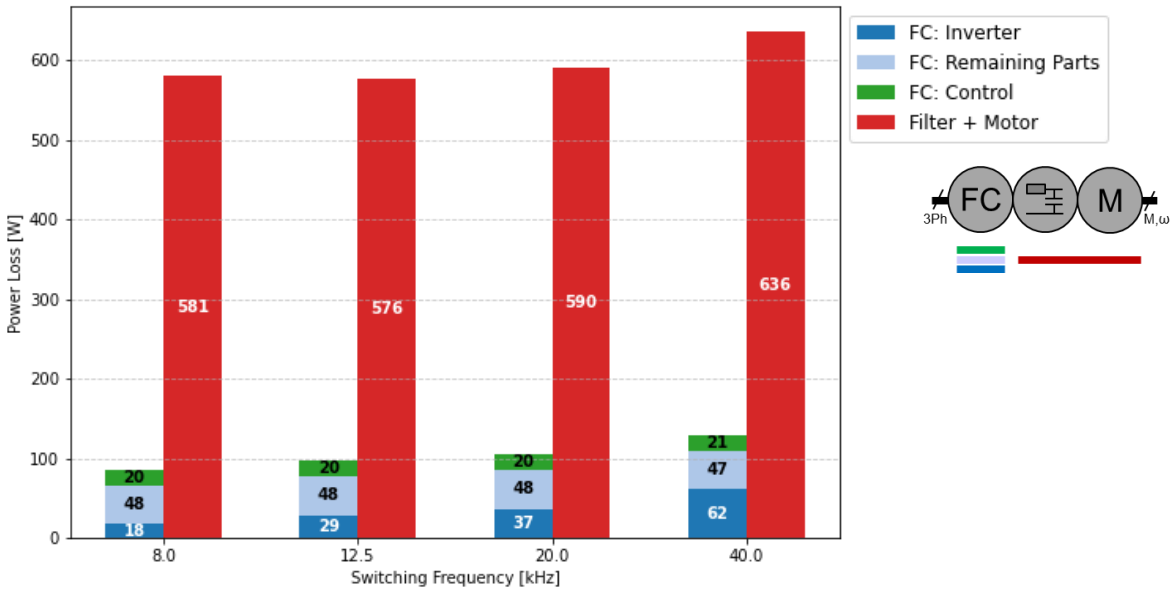


Figure 42: Breakdown of PDS power losses and their evolution with the switching frequency of the inverter. The distribution into the partial losses is based on the measurement of the total PDS losses and simulated and calculated part losses, where the uncertainty is unknown and therefore not shown. In addition, this uncertainty could not be assigned to either the converter or the filter and motor losses.
Operation point: 100 % of nominal shaft speed, 100 % of nominal shaft torque.

From Figure 41 and Figure 42 (dark blue coloured bars) it can be seen that the additional losses come mostly from the rising switching losses of the inverter, while the filter and motor losses do not increase significantly for switching frequencies below 20 kHz. However, switching the inverter at 20 kHz and above significantly increases the losses in the filter and motor, visible in the red bars. Further investigations would be necessary to identify the root cause.

Based on the present knowledge of the system, the following assumption is made: As seen in Figure 16, the inductance of the Grundfos filter decreases for frequencies up to 10 kHz and starts to decay for frequencies higher. On the other hand, for the filter with Kool-Mu core, the inductance stays stable up to approximately 100 kHz, but the capacitor changes significantly for frequencies higher than 10 kHz. Both the decrease of the inductance and the capacitance shift the corner frequency of the filter to higher frequencies, which results in less damping of the current ripple. Figure 43 shows the transfer function of each phase of the three-phase filter with Kool-Mu core material. Since the low pass filter characteristic shows significant change for frequencies higher than 20 kHz, it is not recommended to use the filter for higher switching frequencies.

In addition, effective resistance rises because of the skin effect. Each of the changes mentioned results in additional losses and could be a reason for higher additional losses in the red bars of Figure 41 and Figure 42.

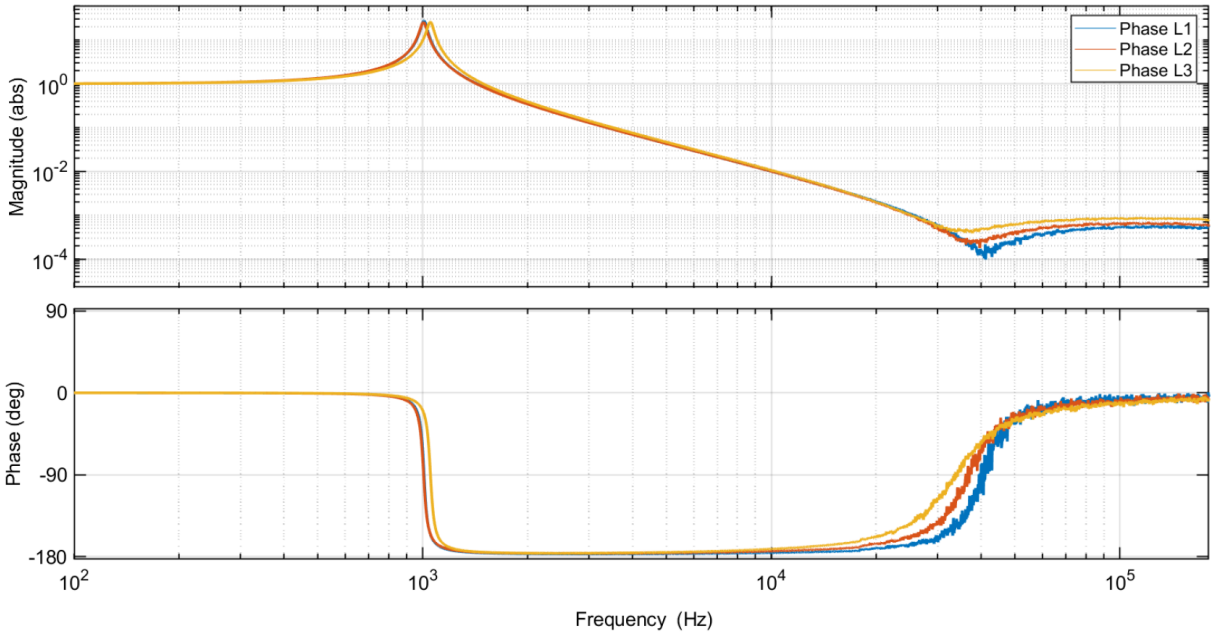


Figure 43: Bode diagram of the three-phase LC low pass filter with Kool-Mu core material.

8.3 SiC VSD without sine filter at different switching frequencies

In this section, the effect of two different switching frequencies is investigated for the mentioned PDS, but without the implementation of any sine filter. The question is, whether the losses saved due to the removed filter are higher than the added losses of the current ripple in the motor and if these losses decrease with higher switching frequency due to a smaller current ripple.

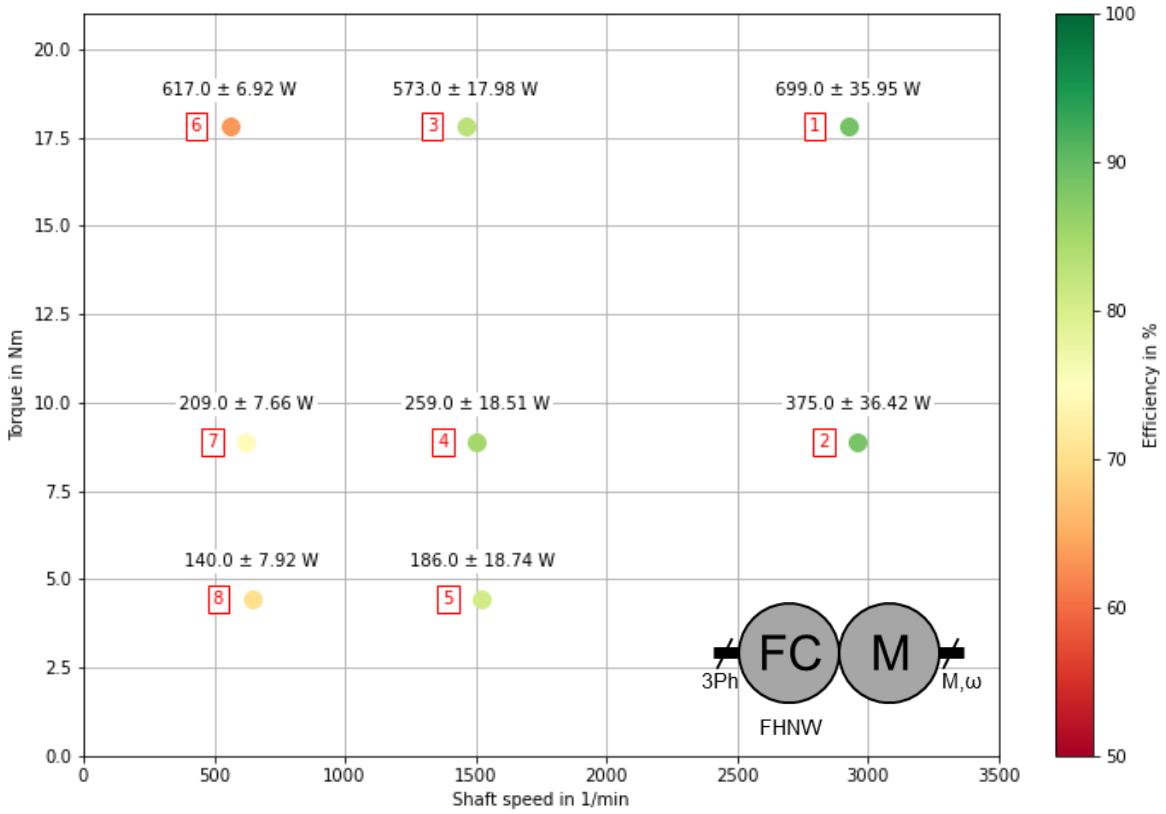


Figure 44: Loss map according to IEC-61800-9-2 of the PDS with the frequency converter developed by FHNW (SiC inverter switched at 8 kHz frequency), without a sine-wave filter and the Grundfos pump motor. The coloured dots are the measured power losses per operation points where the colour corresponds to the efficiency of the system according to the bar on the right.

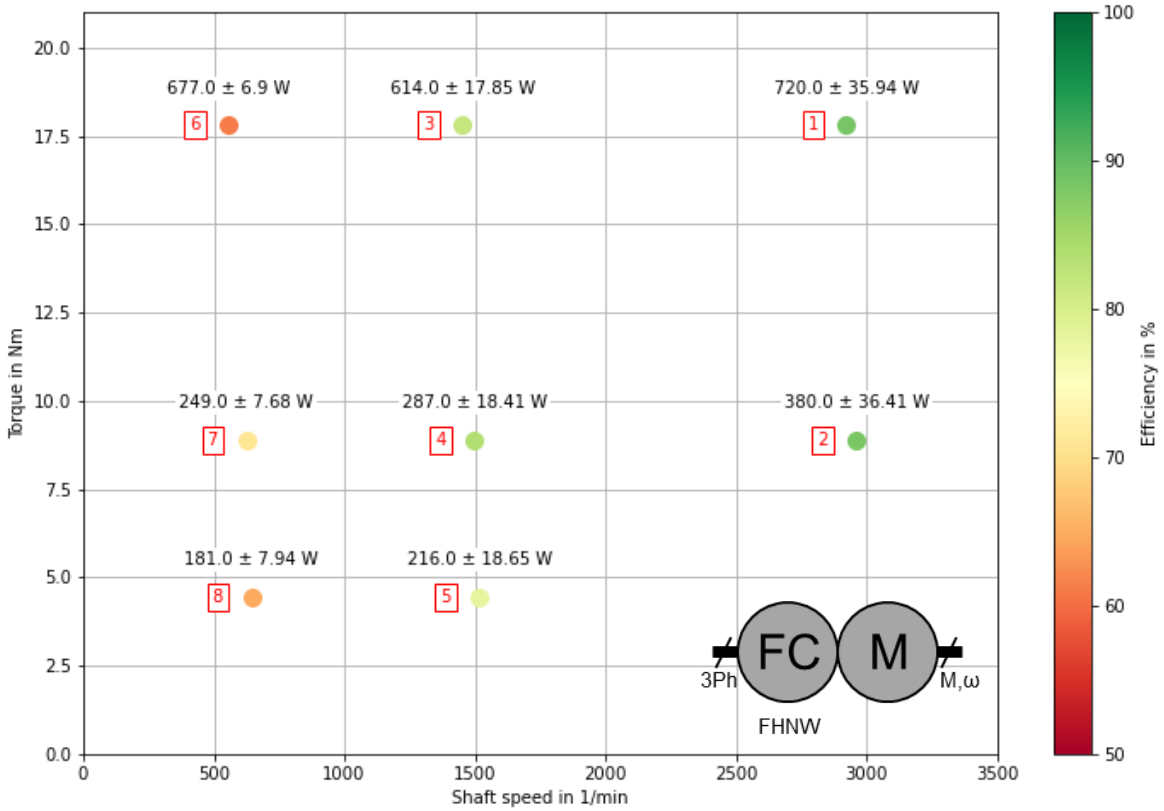


Figure 45: Loss map according to IEC-61800-9-2 of the PDS with the frequency converter developed by FHNW (SiC inverter switched at 20 kHz frequency), without a sine-wave filter and the Grundfos pump motor. The coloured dots are the measured power losses per operation points where the colour corresponds to the efficiency of the system according to the bar on the right.

From the measurement results, presented in the figures above, it can be concluded that the power losses increase with increasing switching frequency. The comparison of Figure 44 with Figure 35 and Figure 36 shows that removing the sine wave filter increases the total power losses. On the other hand, the comparison with the results displayed in Figure 34, shows that the total power losses are still significantly lower than the system using a frequency converter with IGBTs and a commercial filter with iron core.

Comment:

Effects of high voltage slopes (dV/dt) of the SiC MOSFETs on bearings and possible degradation of isolation material were not part of this study.

8.4 Conclusion

The investigations show that a change of the components from IGBT inverter and conventional filter with iron core material to a filter with Kool-Mu material and an inverter with SiC MOSFETs switched at rather low switching frequencies results in the highest gain in efficiency over the entire range of operation points. The effective power loss saving per operation point are displayed in Figure 46.

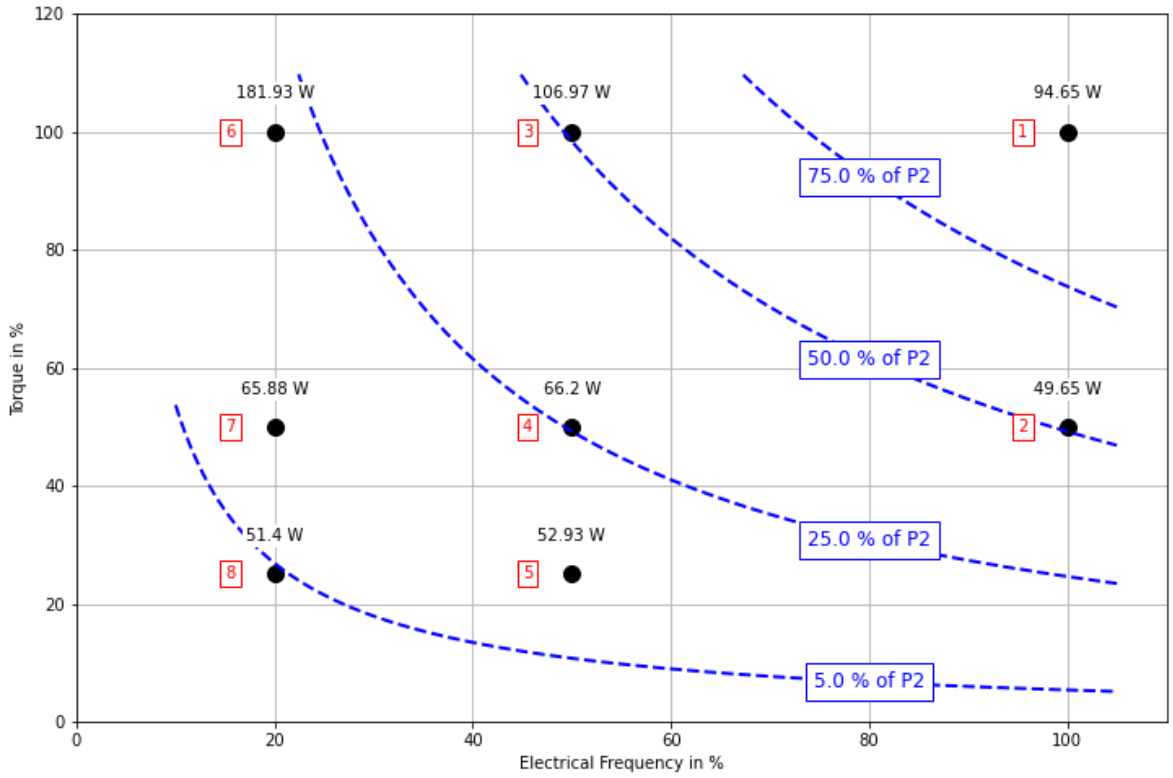


Figure 46: Black dots: Power loss differences per operation point of PDS with frequency converter and sine filter of Grundfos compared to the PDS with SiC frequency converter, switched at 8 kHz and sine filter with Kool-Mu core material. Blue lines: Mechanical power at the shaft in relation to the nominal power of the system.

Independent of the operation point, the losses that can be saved are 50 W at minimum and can be as high as 180 W. The annual energy saving of a PDS of an application can be calculated in case the load profile is known (operation points and its duration). This is done in Chapter 0 to estimate the global energy saving potential for pump systems.

Energetic considerations of Si and SiC pump drives

Parts of this chapter summarise the results of a semester project in the Energy and Environmental Engineering program at the FHNW. Details can be found in the project's technical report [15].

9.1 Calculating energic losses for given mission profiles

According to IEC 61800-9-1 [8], the power losses of a drive system ('PDS'; measured between grid mains and motor shaft) are determined at 8 specific operating points (see also Chapter 2.2).

A real drive system operates according to a load profile, i.e. motor speed and torque, both as a function of time. To calculate the energy consumption, it is therefore useful to establish a frequency distribution of the operating points approached over a certain period of time (e.g. 1 year), similar to Figure 50 further below. The operating points approached in the real profile are not necessarily identical to the points characterised in the loss measurement in IEC 61800-9-1. For this reason, IEC 61800-9-1 proposes a method for estimating the power loss at any operating point (torque / speed) by two-dimensional linear interpolation between the neighbouring measuring points.

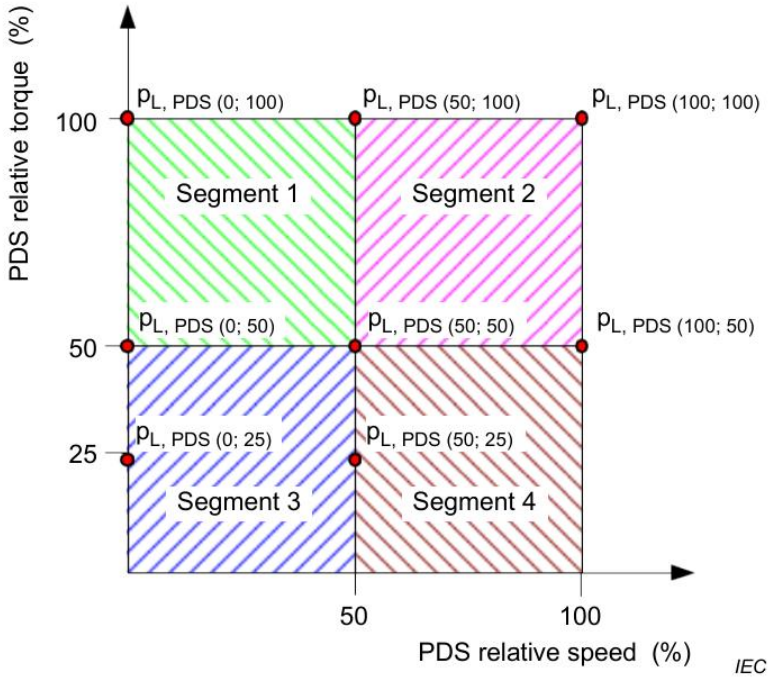


Figure 47: Four segments of deviating operating points of a PDS [8]. The two-dimensional linear interpolation to a specific operating point is done within the segment where this point is located.

Calculating the power loss $P_{L,z}(n_Z, t_Z)$ at a specific operating point Z (n_Z, t_Z):

(quoted from [8], section 7.3.3)

"Interpolation between four defined points A, B, C and D in Figure 48 at an operating point Z

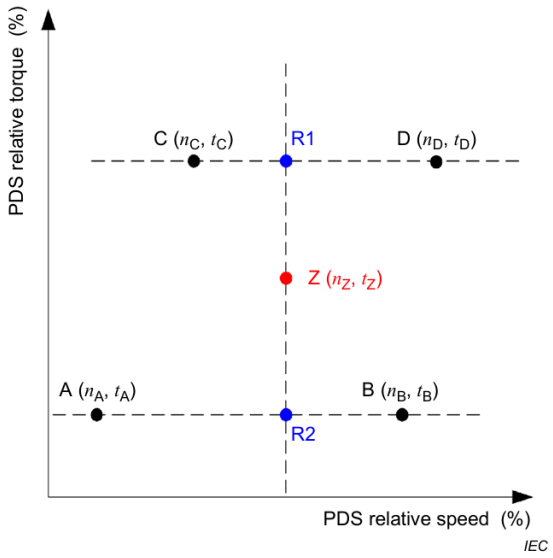


Figure 48: Two-dimensional interpolation for deviating operating points [8].

In the first step, a linear interpolation between points C and D is calculated for the point $R1$. The horizontal component (speed) n of $R1$ is chosen equivalent to the horizontal component n_Z of the required operating point Z. Since the vertical component (torque) of the points C and D are identical ($t_C = t_D$), the losses at the point $R1$ are a function of the horizontal component n_Z only and will lead to $P_{L,R1}(n_Z)$.

In the second step, the losses are interpolated in the same way for the point $R2$. This will lead to $P_{L,R2}(n_Z)$.

In the third step, the losses in the operating point Z are finally calculated by interpolation between $R1$ and $R2$. As $R1$ and $R2$ have the same horizontal component n_Z by definition, this interpolation is a function of the vertical component t_Z only. This will lead to $P_{L,Z}(n_Z)$.

Inserting the values to the equation below gives the final calculation of the losses at the operating point Z.

$$P_{L,Z}(t_Z) = p_{L,R2} + \frac{p_{L,R1} - p_{L,R2}}{t_{R1} - t_{R2}} \cdot (t_Z - t_{R2})$$

In case the motor system contains a motor starter or softstarter, the calculation shall take the same value for both operating points out of Figure 4.

In case the abscissa of the operating point Z at which the losses are desired is less than 25 % speed, the losses shall be determined by linear interpolation using the reference points at 25 % speed."

Calculating the electric energy consumption E_{el} for a given speed and torque profile:

At each operating point $Z(n_Z, t_Z)$, the electric power $P_{el,Z}$ a drive system draws from the grid equals to the mechanical output power plus the power loss:

$$P_{el,Z} = P_{mech,Z} + P_{L,Z} = \left(t_Z \cdot \frac{2\pi}{60} \cdot n_Z\right) + P_{L,Z}$$

The considered mission profile has the time duration T. Within T, m different operating points Z_i, respectively at speed n_i and torque t_i, are approached for their respective time duration Δt_i. The duration of the entire mission profile is the sum of all time periods at the individual operating points:

$$T = \sum_{i=1}^{m} \Delta t_i$$

The electric energy E_{el} consumed by the drive system within one mission profile is:

$$E_{el} = \sum_{i=1}^{m} P_{el,Z_i} \cdot \Delta t_i$$

If the mission profile repeats itself x times within a time period of interest (e.g. 1 year), the total electric energy consumption within this time period is $x \cdot E_{el}$.

9.2 Determination of real pump operating profiles

To gain an understanding of the typical operating modes of speed-controlled pumps, the electrical energy drawn from the grid by two speed-controlled pump systems at the FHNW Brugg-Windisch campus was recorded over a period of approx. 1 month. The pumps are used as

- **Pressure booster pump:** This maintains the system pressure of the drinking water network in Building 1. The system consists of two pumps, each with a motor, each of which is speed-controlled with an associated frequency converter (Figure 49, left).
- **Heating water circulation pump:** This is part of the heating system and supplies hot water from Building 1 to Building 4, approx. 150 metres away on the campus (Figure 49, right).



Figure 49: Pressure booster system in building 1 (left); heating water circulation pump in building 1 (right).

The rated electrical power of each of the two pressure booster pumps is 6.6 kW. The consumption measurements showed that this maximum output was almost never reached. Instead, the power drawn from the grid is predominantly around 2.5 kW (Figure 50).

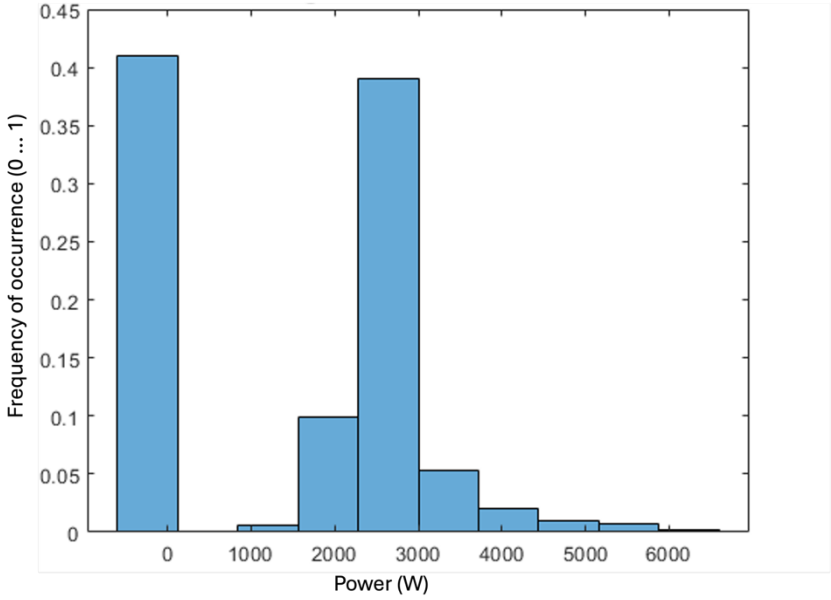


Figure 50: Frequency distribution of the electrical power drawn from the mains by one of the two booster pumps, including off state (left column). The pump is switched off approx. 40% of the time, during which time the second pump in the system is active. When the pump is switched on, the output is <50% of its rated output, with a few exceptions.

The nominal electrical power of the circulation pump is 16.3 kW (specified on the frequency converter). During the measurement campaign, it was found that the circulation pump was operated at an almost constant electrical output over the entire measurement period (Figure 51), which corresponds to approximately 36% of the nominal output.

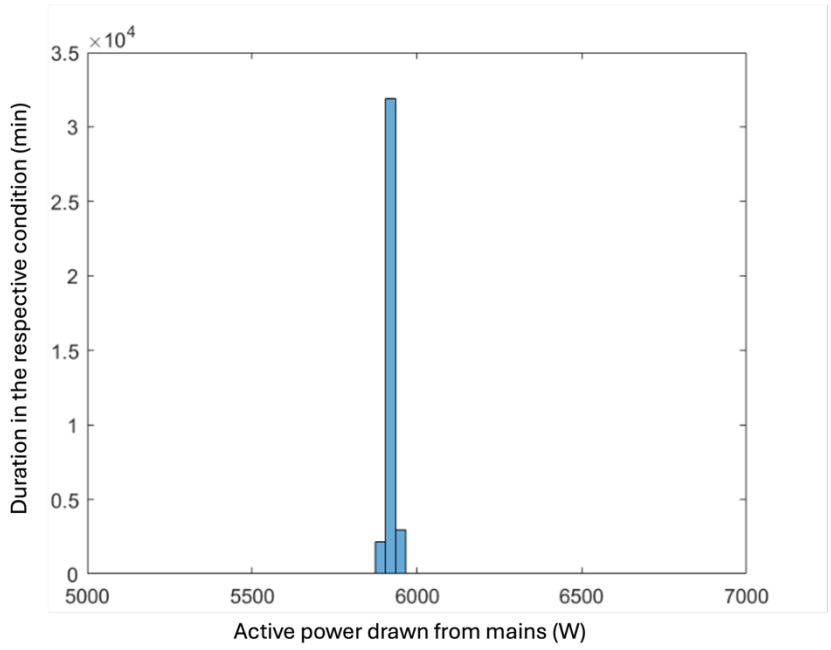


Figure 51: Frequency distribution of the electrical power of the circulation pump drawn from the mains. The pump (and therefore the frequency inverter) runs permanently in the partial load range of approx. 36% of the nominal output.

Conclusion:

- Both speed-controlled pumps analysed - and therefore their frequency converters - are almost always operated at partial load. Typical operating points are < 50 % of the rated power.
- The two pumps were selected at random for this study. Due to the wide variety of pump types, sizes and applications, the measurement results cannot be generalised. For the estimation of the global energy saving potential of SiC pump drives, a typical operating point of 50 % of the nominal power is assumed as an example, which appears plausible based on the measurements carried out.
- If the efficiency of a speed-controlled pump system is increased in the performance range in which the system is most frequently operated, this can have a major effect on energy consumption in real operation. This particularly applies to systems that run around the clock.

9.3 Global energy demand of speed-controlled pumps

In 2011, the International Energy Agency (IEA) compiled an estimate of the electrical energy converted globally in various sectors and drive systems ([16]; Figure 52).

Table 17: Estimated global motor electricity demand by sector and application (2006)

Sectors	Total demand of electric motors (TWh/year)	Pumps		Fans		Compressors		Mechanical movement	
		Demand (TWh/yr)	Sector motor share	Demand (TWh/yr)	Sector motor share	Demand (TWh/yr)	Sector motor share	Demand (TWh/yr)	Sector motor share
Industry	4 488	942	21%	718	16%	1 122	25%	1 705	38%
Commercial	1 412	223	16%	339	24%	603	43%	247	18%
Agricultural	101	20	20%	20	20%	20	20%	40	40%
Transport	159	16	10%	16	10%	48	30%	80	50%
Residential	**948**	**142**	**15%**	**237**	**25%**	**474**	**50%**	**95**	**10%**
Total	**7 108**	**1 344**	**18.9%**	**1 330**	**18.7%**	**2 267**	**31.9%**	**2 167**	**30.5%**

Sources: De Almeida *et al*, 2008b; A+B International, 2009.

Figure 52: Extract of the determined energy consumption values from [16].

Figure 52 shows the value of 1,344 TWh/year for the global electrical energy demand of all pumps for the year 2006. This value includes all pumps of all performance classes, with and without frequency converters (FC). Regarding frequency converters, the IEA report estimates that the proportion of drives with frequency converters is approx. 30 %, which refers to the drives sold in Germany at that time (2011), which were sold directly with a frequency converter.

The proportion of drives with frequency converters has presumably risen since 2011; however, a still conservative value of 40 % is assumed for the estimates carried out here.

Furthermore, the global annual energy consumption of pumps has presumably risen since 2006. If we assume an annual growth rate of 2 % between 2006 and 2025, the energy consumption of pumps would be 45 % higher than the 1,344 TWh/year claimed above, namely 1,948 TWh/year. However, since annual growth rates are not known, a possible range of the global annual energy consumption by speed-controlled pumps is used in the following. The lower limit of the range being the figures of 2006; and the upper limit including an annual growth rate of 2 % since then:

Lower limit: $1'344\,\frac{TWh}{year} \cdot 40\% \approx 538\,\frac{TWh}{year}$

Upper limit: $1'948\,\frac{TWh}{year} \cdot 40\% \approx 779\,\frac{TWh}{year}$

9.4 Conversion of power to torque and speed for hydraulic systems

As the annual energy consumption of speed-controlled pumps is roughly known, the next steps towards the energy saving potential of more efficient SiC frequency inverters are made.

Due to non-existent data, the following assumptions are made:

1. All currently installed frequency inverters are based on silicon technology (e.g. IGBTs).
2. All currently installed frequency inverters are converted to more efficient SiC technology.
3. The operating point of the frequency inverters is 40 % of the rated power (see section 9.2).

Assumption 3 is very simplistic; due to the lack of more precise data available, this assumption is considered a 'best guess'. Furthermore, only the power value of 40 % of the nominal power is specified. Realistic torque and speed values must be derived from this. This is done briefly below:

According to IEC 61800-9-1, the torque t required by the hydraulic load of a pump is quadratic to the angular speed $t \propto \omega^2$ of the motor shaft:

$$t \propto \omega^2 \;\Rightarrow\; t = \alpha \cdot \omega^2$$

Mechanical power is the product of torque and angular velocity, $P_{mech} = t \cdot \omega$. For a hydraulic system, P_{mech} is hence proportional to the third power of ω:

$$P_{mech} = \alpha \cdot \omega^3$$

This relation can be transferred to the nominal operating point (nominal torque t_N, nominal speed ω_N):

$$P_{mech,N} = \alpha \cdot \omega_N^3$$

The values $P_{mech,N}$ and ω_N can be looked up on the nameplate of any motor. The constant α can then be derived from the known values $P_{mech,N}$ and ω_N:

$$\alpha = \frac{P_{mech,N}}{\omega_N^3}$$

For the motor used in this project, $P_{mech,N} = 5500\,W$ and $n_N = 2940\,min^{-1} \Rightarrow \omega_N = 307.8\,rad/s$ (see Table 7). This gives:

$$\alpha = 1.886 \cdot 10^{-4}\,W \cdot s^3$$

In assumption 3 above, the operating point of 40% of the rated power should be used. Considering the equations above, the motor speed of a hydraulic pump at 40% of the rated power is:

$$\frac{\omega_{40\%}}{\omega_N} = \sqrt[3]{0.4} \approx 0.737$$

With the value of α of the used motor, the torque at 40% power can be calculated:

$$t_{40\%} = \alpha \cdot \omega_{40\%}^2 = 1.886 \cdot 10^{-4}\,W \cdot s^3 \cdot (0.737 \cdot 307.8\,rad/s)^2 = 9.7\,Nm = 0.545 \cdot t_N$$

The resulting operating point relevant for the energetic calculations is shown in Figure 53.

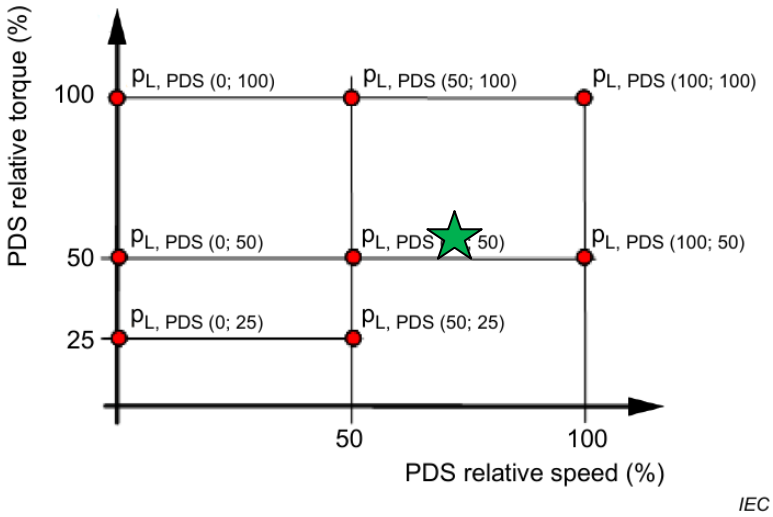


Figure 53: The operating point of a hydraulic system at 40% ($P_{mech,N}$) is at 73.7% of nominal speed and 54.5% of nominal torque (green star).

9.5 Energy and cost saving potential per 5.5 kW system

Taking the measured efficiencies of the Grundfos IGBT drive and the FHNW SiC drive (see chapter 0), annual energy consumptions have been calculated for both systems at the operating point 40 % ($P_{mech,N}$), as explained in section 9.4. The results are shown in Table 11 below.

Table 11: Energetic comparison between the Grundfos IGBT drive (using Grundfos sine filter) and the FHNW SiC drive (using the Kool-Mu filter). Switching frequency of both inverters: 8 kHz. Operating point at 40 % of rated power, respectively. The displayed values may contain slight inaccuracies due to rounding.

	Grundfos IGBT drive	FHNW SiC drive
Motor speed (min^{-1})	2167	2167
Torque (Nm)	9.7	9.7
P_{mech} at motor shaft (kW)	2.20	2.20
P_{el} drawn from grid (kW)	2.56	2.48
Efficiency from grid mains to motor shaft	85.9 %	88.7 %
Annual energy consumption (kWh)	22,450	21,722
Annual energy savings (kWh)	**-**	**727**
Annual energy cost (CHF)[1]	4,490.00	4,344.52
Annual cost reduction (CHF)	**-**	**145.48**

Assuming a purchase price of CHF 300 higher for a new SiC drive compared to an IGBT drive, the higher initial costs are amortised after approx. 2 years.

[1] Calculated with an energy price of 0.2 CHF / kWh.

9.6 Annual global energy saving potential of SiC pump drives

In section 9.3 the global annual consumption of electrical energy by speed-controlled pumps has been estimated to 538 ... 779 TWh/year. If we assume that all these drives are operated at 40 % of their rated power with an IGBT inverter and have an efficiency of $\eta_{IGBT} = 85.9\ \%$ at this operating point (Table 11), their annual combined mechanical output energy is:

$$E_{mech\ ,global,year} = (538\ TWh \ldots 779\ TWh) \cdot 85.9\% = 462 \ldots 669\ TWh$$

This energy remains the same even if the technology is changed, as it is given by the applications.

The energy loss of drives with IGBT technology is therefore:

Lower limit: $E_{loss,IGBT,global,year} = 538\ TWh - 462\ TWh = 76\ TWh$

Upper limit: $E_{loss,IGBT,global,year} = 779\ TWh - 669\ TWh = 110\ TWh$

The power consumption of SiC drives can be calculated from the energy required at the motor and the efficiency of a SiC drive ($\eta_{SiC} = 88.7\%$; Table 11):

Lower limit: $E_{SiC,global,year} = \frac{E_{mech\ ,global,year}}{\eta_{SiC}} = \frac{462\ TWh}{88.7\%} = 521\ TWh$

Upper limit: $E_{SiC,global,year} = \frac{E_{mech\ ,global,year}}{\eta_{SiC}} = \frac{669\ TWh}{88.7\%} = 754\ TWh$

The annual global energy saving potential can finally be calculated as the difference between the power consumption of Si drives and more modern SiC drives:

Lower limit: $\boldsymbol{E_{GlobalSaving} = 538\ TWh - 521\ TWh = 17\ TWh}$

Upper limit: $\boldsymbol{E_{GlobalSaving} = 779\ TWh - 754\ TWh = 25\ TWh}$

As a comparison:

17 ... 25 TWh approximately corresponds to the yearly electric energy output of 2-3 large thermal power plants with constant output power around 1 GW and 100% availability.

Online tool for energetic calculations

10.1 Intended purpose

In their applications, electric drive systems are typically operated within a certain load profile to supply their application. The load profile is the speed and torque at the motor shaft as a function of time.

Manufacturers of drive systems often provide efficiency or energy loss data according to a standard. This can be EN 61800-9-1 which contains only eight operating points. These eight points often do not directly correspond with the operating points of the user's application. Furthermore, the drive system may be operated at varying load. This makes it difficult for the user to estimate the system's energy consumption and resulting energy cost. Also, comparisons between different drives are difficult.

The purpose of the tool developed here is to estimate the energy consumption and energy cost of a drive system, when the user provides minimal information. The functions are therefore:

- Calculate the annual energy consumption of a drive system when the user provides efficiency data and a load profile.
- Calculate the annual energy cost.
- Compare the annual energy consumptions and energy costs of two different drive systems for the same application.
- Support the user of a drive system in his decision to switch to a more efficient drive system.

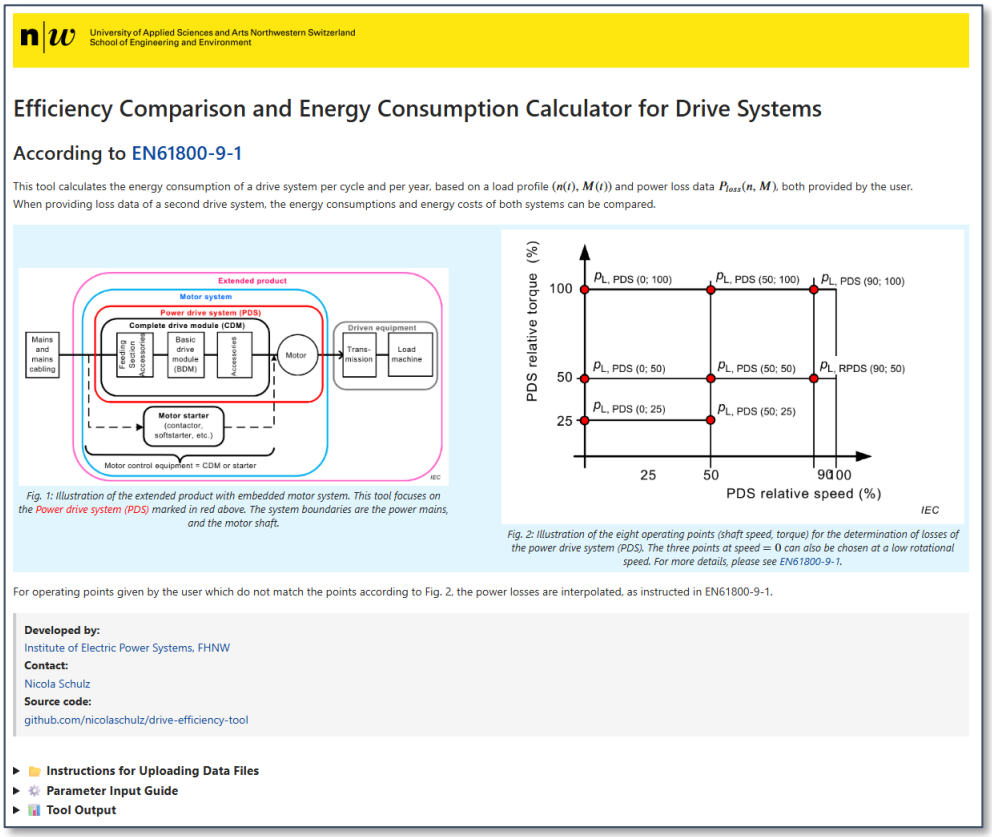


Figure 54: Screenshot of the online calculation tool which calculates energy consumption and energy cost of a drive system when the user enters efficiency data, electricity cost and a load profile.

The tool can be either downloaded (Jupyter notebook format) or directly used online at:

https://github.com/nicolaschulz/drive-efficiency-tool

The source code is open and can be modified according to the user's requirements.

10.1 Implementation and functions

The instructions for using the tool are provided in the tool's user interface. The user must provide the following data:

- Loss map of one or two drive systems (PDS) according to EN 61800-9-1 (Excel format)
    - Alternatively, if no data according to EN 61800-9-1 is available: Losses as a function of the output power for one or two drive systems (Excel format)
- Load profile of the drive system: speed (min^{-1}) and torque (Nm) in single time steps (Excel format). The duration of a time step can be set in the tool's user interface.
    - Alternatively: Output power in single time steps (Excel format)
- Electricity cost (CHF / kWh)
- Nominal speed and nominal torque of the motor.

Example Excel files can be downloaded.

Figure 55 shows a screenshot of the output. Additionally to the graphical plots, several calculations are carried out, e.g.:

- Energy consumption and energy cost of one or two drive systems within one execution of the provided load profile.
- Energy and cost savings when changing to the more efficient drive system within one execution of the provided load profile.
- The corresponding values as above, but annually, when the load profile is continuously repeated within one year.

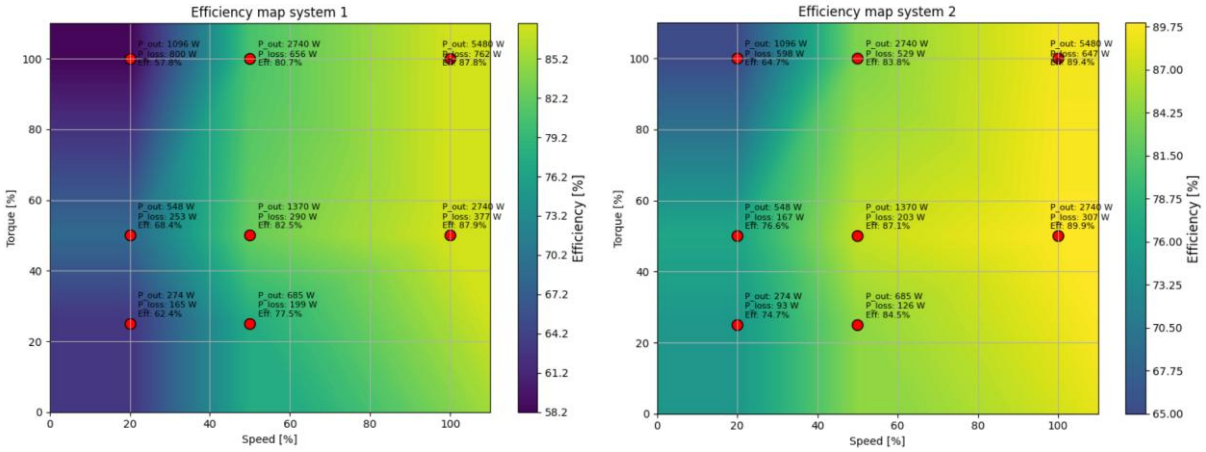


Figure 55: Example output of the tool. Left: Efficiency map of the Grundfos PDS (chapter 7.4); right: efficiency map of the FHNW SiC PSD (chapter 7.6).

Conclusions and outlook

11.1 Conclusions

A systematic comparison between a commercial 5.5 kW IGBT-based drive system for pump applications and a newly developed SiC MOSFET-based drive system designed at the FHNW is provided. The efficiencies of both systems were assessed according to IEC 61800-9-1 which includes operation points at partial load efficiency, being relevant for many application cases. Efficiency measurements were conducted on complete systems, from grid connection to motor shaft.

The custom-developed SiC drive system incorporated state-of-the-art components including a Si-based rectifier module, a 3-phase 2-level SiC MOSFET inverter, and a sine-wave output filter based on Kool-Mu magnetic material. The efficiency measurements of both systems were carried out on a dedicated test bench for drive systems to be tested according to IEC 61800-9-1 and using a high precision power analyser to record the efficiency data.

Key findings from the comparative study:

- The SiC-based drive system showed a clear efficiency advantage over the entire load range, particularly at partial load. Its efficiency advantage compared to the IGBT system ranged from 1.3 percentage points at nominal load to 10 percentage points at partial load.
- The optimal efficiency of the SiC drive was achieved at the lowest tested switching frequency of 8 kHz. Increasing the switching frequency increased losses, in the inverter as well as in the magnetic components (filter + motor).
- A major part of the system losses occurs in the motor-side filter and in the motor. The distribution of losses between filter and motor was not analysed. It is assumed that by an updated filter design (different capacitors), the losses could be further reduced.
- The SiC-based frequency converter is not more complex to implement than a conventional IGBT inverter. For conservative designs (e.g. regarding voltage slopes), SiC MOSFETs can be operated at dV/dt rate similar to that of IGBTs, since the inverter only contributes a small fraction to the total drive system losses.
- Based on the measured loss data, an extrapolated global analysis was carried out. It was estimated that replacing conventional IGBT-based drives with SiC-based systems in pump applications could yield global annual energy savings of approximately 17 to 25 TWh.

To support end users in evaluating the energetic performance of their own systems, a web-based calculation tool was developed. This tool allows users to input operational profiles and system-specific efficiency data to estimate energy consumption and compare alternative drive solutions.

These results highlight the technical and environmental benefits of adopting SiC-based drive systems and underline the importance of user-accessible tools to facilitate energy efficiency improvements in industrial applications.

11.2 Outlook

In this project, it was demonstrated that the efficiency of drive systems in the kW power range can be clearly improved by using SiC MOSFETs instead of IGBTs in the inverter. There remains only little potential for further substantial efficiency improvements of drive systems when only improving the inverter efficiency itself. This becomes clear when considering that the largest proportion of losses occurs in the motor (Figure 41 and Figure 42).

In the SFOE project “Roadrunner” [17] it was shown that motor losses can be reduced using an inverter in multi-level topology to drive the motor. In comparison to two-level topology, the losses in the motor due to harmonic currents could be reduced by 75% by using a three-level topology. In the “Roadrunner” project, IGBTs were still used in the inverter.

The next logical step is therefore to combine the efficiency benefits of SiC in the inverter with the advantages of a multilevel topology for motor efficiency. For this reason, the so-called dual inverter (DI) topology, in which the motor is operated by two inverters, each in standard topology, appears to be interesting [18]. Three-level operation can be achieved by appropriately configuring and operating the two individual inverters.

In the follow-up project ‘MuSiC’, which has already been launched, the advantages of a SiC dual inverter regarding the efficiency of drive systems and how it compares to other topologies are to be investigated.

National and international cooperation

The FHNW collaborated with two industrial partners in OPTIPUMP, whose roles are briefly described below:

12.1 Grundfos Pumpen AG

Grundfos Pumpen AG (Swiss branch in Fällanden, CH) is a leading global supplier of pumps in various performance classes and for different applications. Its products also include speed-controlled pumps via a frequency converter. Grundfos is providing the FHNW with the complete pump drive system described in Chapter 0 for this project. Grundfos has been interested in how speed-controlled pump drive systems can be made more energy-efficient.

12.2 Plexim GmbH

Plexim GmbH (Zurich) offers the PLECS software tool for the simulation of power electronic systems. In addition to the electrical domain, simulations can also be carried out in the thermal, magnetic and mechanical domains to fully map an entire system. PLECS simulations can be used to dimension power converters or even complete drive systems (semiconductor types, cooling, etc.), estimate energy losses and develop control algorithms. PLECS is now a standard simulation tool for power electronics in both the academic and industrial sectors. Plexim has supported the FHNW in developing the simulation model described in chapter 5.2.

Publications and other communications

Publications so far:

- OPTIPUMP yearly project reports 2022, 2023, 2024: https://www.aramis.admin.ch/Grunddaten/?ProjectID=50642
- Energetic calculation tool for drive systems: https://github.com/nicolaschulz/drive-efficiency-tool

Planned:

- Publication of the main project results in an application-oriented power electronics journal such as Bodo's Power Systems or similar (foreseen in 2025)

References

[1] «SiCUm – Grundlagen eines effizienten SiC Umrichters im Niederspannungsbereich», Swiss Federal Office of Energy, 2021, project no. SI/501732, https://www.aramis.admin.ch/Grunddaten/?ProjectID=41493

[2] M. Makoschitz et al., “Wide Band Gap Technology: Efficiency Potential and Application Readiness Map”, 4E Power Electronic Conversion Technology Annex (PECTA), May 2020.

[3] International Electrotechnical Commission, IEC 61800-9-2:2023 - Adjustable speed electrical power drive systems (PDS) – Part 9-2: Ecodesign for motor systems – Energy efficiency determination and classification*, 2nd ed., Geneva, Switzerland: IEC, 2023.*

[4] Grundfos product website (Nov. 2022): Norm pump NK 32-160/177AA2F2AESBQQELW1, https://product-selection.grundfos.com/ch/products/nk-nke-nke-series-2000-nk-bare-shaft/nk/nk-32-160177-98973410?tab=variant-curves

[5] Grundfos product website (May 2025): Frequency converter CUE 3X380-500V IP20 5,5KW, https://product-selection.grundfos.com/ch/products/cue-1/cue/cue-3x380-500v-ip20-55kw-99616714?tab=variant-specifications&pumpsystemid=2662864746

[6] Grundfos product website (May 2025): Sine-wave filter, https://product-selection.grundfos.com/us/products/cue-1/cue-accessories/sine-wave-filter-96754976?pumpsystemid=2657826475&tab=variant-specifications

[7] Grundfos product website (May 2025): Motor MG132SC, https://product-selection.grundfos.com/us/products/mg-ml/mg132sc-85187322?pumpsystemid=2676374529&tab=variant-specifications

[8] International Electrotechnical Commission, IEC 61800-9-1:2017 - Adjustable speed electrical power drive systems – Part 9-1: Ecodesign for power drive systems, motor starters, power electronics and their driven applications – General requirements for setting energy efficiency standards for power driven equipment using the extended product approach (EPA) and semi analytic model (SAM)*,* 1st ed., Geneva, Switzerland: IEC, 2017.

[9] Universal Elektronik Import (UEI) website (May 2025), https://uei-vienna.com/produkte/hioki-pw8001-power-analyzer/

[10] HIOKI website (May 2025): Power Analyzer PW8001, https://www.hioki.com/global/products/power-meters/power-analyzer/id_412384

[11] MTS website (May. 2025): Dual-Range Torque sensor Type 4503B, https://www.mts.ch/produkte-messtechnik-schaffhausen-gmbh/drehmomentsensoren/zweibereichs-drehmomentsensoren-typ-4503b.html/105

[12] International Electrotechnical Commission, IEC TS 60034-31:2021 - Rotating electrical machines – Part 31: Selection of energy-efficient motors including variable speed applications – Application guidelines*,* 2nd ed., Geneva, Switzerland: IEC, 2021.

[13] L. Müller and R. Suter, “Filterentwicklung für hocheffiziente SiC Antriebssysteme”, Bsc. thesis, FHNW, August 2023.

[14] Magnetics Inc. website (May 2025): Kool-Mu Cores, https://www.mag-inc.com/Products/Powder-Cores/Kool-Mu-Cores

[15] C. Oxé, “Energiesparpotential von effizienteren Pumpensystemen”, semester project report, FHNW, June 2023.

[16] P. Waide and C. U. Brunner, «Energy-Efficiency Policy Opportunities for Electric Motor-Driven Systems,» International Energy Agency, Paris, 2011.

[17] “Roadrunner - Commerical Vehicle Inverter and Testing on eBus Line”, Swiss Federal Office of Energy, Project no. SI/501891, https://www.aramis.admin.ch/Texte/?ProjectID=44239.

[18] M. Thommen, “PCB-based Inverter for Open Winding Induction Machine”, MSc. Thesis, FHNW, 2024.